University of California, Irvine
Henry Samueli School of Engineering
Department of Mechanical and Aerospace Engineering

Computational Environmental Sciences Laboratory

Principal Investigator: Donald Dabdub, Ph.D.*

Chlorine Emissions from Activated Sea-Salt Aerosols and Their Potential Impact on Ozone

FINAL REPORT

Eladio M. Knipping and Donald Dabdub

Prepared for the California Air Resources Board and the California Environmental Protection Agency

ARB Contract No. 00-324

* Contact Information
Phone: 949-824-6126; Fax: 949-824-8585
email: ddabdub@uci.edu
http://albeniz.eng.uci.edu/dabdub

March 8, 2002

The statements and conclusions in this Report are those of the contractor and not necessarily those of the California Air Resources Board. The mention of commercial products, their source, or their use in connection with material reported herein is not to be construed as actual or implied endorsement of such products.

The authors acknowledge the following persons for providing assistance, discussions, information and/or data pertaining to this research (in alphabetical order): David Allen (University of Texas, Austin), Cort Anastacio (University of California, Davis), Kelly BéruBé (Cardiff University), Joe Cassmassi (South Coast Air Quality Management District), Elaine Chapman (Pacific Northwest National Laboratories), Gerrit De Leeuw (TNO Physics and Electronics Laboratory, Netherlands), Barbara J. Finlayson-Pitts (University of California, Irvine), Robert Griffin (Duke University), Matthew P. Fraser (Rice University), Michael Kleeman (University of California, Davis), Curt Miller (South Coast Air Management District), Jason Rogge (University of California, Irvine) and John H. Seinfeld (California Institute of Technology). The research presented in this report has not been subjected to review from these persons, and therefore does not necessarily reflect their views; their acknowledgement is not to be construed as endorsement.

This Report was submitted in fulfillment of ARB Contract No. 00-324: "Chlorine Emissions from Activated Sea-Salt Aerosols and Their Potential Impact on Ozone" by The University of California, Irvine, under the sponsorship of the California Air Resources Board. Work was completed as of January 8, 2002.

Table of Contents

List of Figures

List of Tables

Abstract

A photochemical modeling study is performed to determine whether urban photochemical models simulating sea-salt particle chemistry can predict observed chlorine levels and how such chlorine levels affect ozone formation. A host urban airshed model, employing a rich chemical mechanism and simulating aerosol dynamics, is augmented with current sea-spray generation functions, a comprehensive gas-phase chlorine chemistry mechanism and several heterogeneous/multiphase chemical reactions considered key processes leading to reactive chlorine formation. Modeling results adequately reproduce regional sea-salt particle concentrations. These particular heterogeneous/multiphase chemical reactions do not affect the rate of hydrochloric acid displacement nor do they enhance aerosol nitrate formation. Chlorine levels in the model are predicted an order of magnitude below observed values, albeit 30 times better than previous studies. The results suggest that inclusion of sea-salt derived chlorine chemistry may increase morning ozone predictions by as much as ~12 ppb in coastal regions and by ~4 ppb to the peak domain ozone in the afternoon. Peak ozone concentrations at most monitoring sites increase by 2 – 4 ppb and even higher ozone increases, up to 7 ppb, are predicted at other times not coinciding with the peak. An emissions inventory of anthropogenic sources of chlorine is recommended as these may enhance ozone formation even further by emitting chlorine gases directly into polluted regions.

Executive Summary

Urban photochemical models have not included chlorine chemical reactions because significant concentrations of its most oxidizing form, chlorine atoms, have not been expected in these regions. Therefore its effect on ozone formation has been estimated as minimal. Indeed, most of the chlorine present in fresh sea-salt particles, the principal atmospheric chlorine reservoir, is released to the gas-phase as hydrochloric acid due to displacement by less-volatile stronger acids *and* the reaction of hydrochloric acid with the hydroxyl radical, the main atmospheric oxidant, to form chlorine atoms is slow. Nonetheless, laboratory studies have shown that sea-salt particles may undergo chemical reactions that lead to the release of photochemical chlorine-atom precursors. Field studies provide evidence supporting the presence of these photo-labile chlorine species in coastal regions. Thus, heterogeneous/multiphase chemical reactions on sea-salt particles may enhance daytime chlorine-atom levels beyond that predicted solely due to the gas-phase reaction of hydroxyl radical with hydrochloric acid.

The California Air Resources Board has expressed interest in determining the influence that sea-salt particles have on air quality. Preliminary simulations performed by the ARB suggested that the chlorine radical could significantly impact predicted ozone concentrations and warranted further study. In order to determine the influence of chlorine chemistry in coastal regions, a systematic modeling study has been performed in order to assess whether urban photochemical models simulating sea-salt particle chemistry can predict observed chlorine levels. In addition, this study determines how such chlorine levels affect the formation of ozone in an urban coastal airshed. The host model used for the current study is based on the Caltech (CIT) Airshed Model. The model employs a newly developed chemical mechanism. Aerosol particles are modeled using an internally mixed assumption, i.e. all particles within a size bin are assumed to have the same composition. A thermodynamics module describes the gas-aerosol partitioning of inorganic aerosol constituents. Open ocean and surf-zone marine aerosol fluxes are calculated using state-of-the-science sea-spray generation functions. A comprehensive gas-phase chlorine chemistry mechanism and several heterogeneous/multiphase chemical reactions considered key processes leading to reactive chlorine concentrations in urban coastal regions are incorporated in to the model. Air quality simulations of conditions on September 8 – 9, 1993 are presented in this study.

Modeling results show that regional twenty-four hour average sodium mass observations are adequately reproduced by the model. Sea-salt concentrations are dominated by the surf-zone production of sea-spray; the open-ocean contribution to coastal sea-salt aerosol concentrations is negligible. Although some sea-salt particles do travel for several tens of kilometers inland, concentrations are quite low beyond coastal regions. The newly added heterogeneous/multiphase chemical reactions do not affect the rate of acid displacement nor do they enhance aerosol nitrate formation. Chlorine levels in the model reach a maximum 1-hour average concentration of 12 ppt, predicted both in the late evening and at pre-dawn, an order of magnitude below observed values. Nonetheless, these predictions represent an increase by a factor of 30 in the ability to reproduce Cl_2 values when compared to previous modeling studies. Addition of a nighttime mechanism of chlorine formation increases Cl_2 predictions to values more consistent with observations. However, the nature of the true nighttime mechanism is still uncertain.

The modeling results suggest that inclusion of sea-salt derived chlorine chemistry in photochemical models may increase morning ozone predictions by as much as ~12 ppb in coastal regions and by ~ 4 ppb to the peak domain ozone in the afternoon. Although the influence dissipates in later hours, the fraction of the basin affected by the chlorine chemistry increases due to the influence of various physicochemical processes, with transport being the dominant process. Peak ozone concentrations at most monitoring sites increases by 2 – 4 ppb and even higher ozone increases, up to 7 ppb, are predicted at other times not coinciding with the peak. Overall, ozone exposure is increased throughout the domain. In addition, anthropogenic sources may also enhance ozone formation by emitting chlorine gases directly into regions rich in hydrocarbons and oxides of nitrogen. Further studies are warranted in order to reduce mechanism uncertainties, refine the parameterization of heterogeneous/multiphase reactions, incorporate external aerosol mixtures and aqueous-phase chemistry, and collect or estimate emission by anthropogenic and other natural non-marine sources.

1. Introduction

1.1 Background

For over a decade, there has been increasing attention on the role of chlorine atoms as potential oxidants of organic compounds in urban coastal areas [*Keene et al.,* 1990; *Finlayson-Pitts,* 1993; *Pszenny et al*., 1993; *Keene et al.,* 1998]. However, urban photochemical models have not included reactions to model chlorine chemistry. The reasoning behind this omission of chlorine chemistry may lay in the belief that significant chlorine atom concentrations do not develop in these regions making the effect on ozone formation minimal [*Jacob,* 2000]. Indeed, the reaction of hydrochloric acid, HCl, with the hydroxyl radical (OH) to form chlorine atoms (Cl) is slow, *and* most of the chlorine present in fresh sea-salt particles, the principal atmospheric chlorine reservoir, is released to the gas-phase as hydrochloric acid due to displacement by less-volatile stronger acids [*Gard et al.,* 1998; *Hughes et al.,* 2000].

Nonetheless, laboratory studies have shown that sea-salt particles may undergo chemical reactions that lead to the release of photochemical chlorine-atom precursors [*Finlayson-Pitts and Hemminger,* 2000]. Field studies have provided evidence supporting the presence of these photo-labile chlorine species in coastal regions. Non-specific measurements of Cl_2*, expected to be primarily molecular chlorine (Cl_2) and some hypochlorous acid (HOCl), up to 254 ppt (≤127 ppt as Cl_2) have been made in coastal air using a mist chamber technique [*Keene et al.,* 1993]. Other investigators have made specific measurements of Cl_2 as high as 150 ppt at a New York coastal site using atmospheric pressure ionization mass spectrometry (API-MS) [*Spicer et al.,* 1998]. Heterogeneous/multiphase chemical reactions on sea-salt particles may enhance daytime chlorine-atom levels beyond that predicted solely due to the gas-phase reaction of hydroxyl radical with hydrochloric acid.

The California Air Resources Board (ARB) has expressed interest in determining the influence that sea-salt particles have on air quality. Recently, the California Air Resources Board conducted a study on the air quality impacts of the use of ethanol in California reformulated gasoline [*California Air Resources Board*, 1999]. In this study, sensitivity simulations were performed to assess the cumulative impact that the addition or variations of several parameters, including chlorine chemistry, may have on air-pollutant

concentrations using various gasoline reformulations. The ARB included a single reaction of ethanol oxidation by the Cl radical (set to a constant basin-wide concentration) inferring that increased oxidation of ethanol by the Cl radical would lead to increased levels of acetaldehyde and PAN. It must be noted that the objective of the study was to compare four different fuel reformulations under worst-case scenarios.

However, those sensitivity simulations cannot determine clearly the influence of Cl chemistry due to several limitations. The sensitivity studies also included a three-fold increase in on-road motor vehicle hydrocarbon and CO emissions, revised rate constants for the OH + ethanol and OH + MTBE reactions, and revised boundary conditions. An exact contribution of the influence of chlorine chemistry could not be decoupled from the other effects. In addition, the sensitivity studies set a constant chlorine-atom concentration of 10^4 molecules cm^{-3}, a value considered on the higher end of estimates for the diurnally-averaged concentration in the marine boundary layer. The use of this value places no dependency on solar irradiation or on location with respect to chlorine sources in the model domain.

Another sensitivity simulation, independent of the ethanol study, was performed by the ARB [*L. Woodhouse, California Air Resources Board*, personal communication]. The 1987 SCAQS episode using 1997 baseline emissions was modeled using the UAM-FCM model with the SAPRC97 chemical mechanism and a SAPRC97 chlorine module consisting of 32 additional gas-phase reactions adapted from *Carter et al.* [1997b]. Setting a constant Cl_2 concentration of 4 ppt throughout the domain, which would photolyze during daylight to form chlorine atoms, the predicted domain peak ozone increased by about 80% compared to the baseline simulation. This result suggested to the ARB that the chlorine radical could significantly impact predicted ozone concentrations and warranted further study.

In order to determine the influence of chlorine chemistry on an urban airshed, we present here the first systematic modeling study that addresses two important issues: First, can urban photochemical models that simulate sea-salt particle formation make first-order estimates of observed chlorine levels? Second, how do such chlorine levels affect the formation of ozone in an urban coastal airshed?

This manuscript begins by exploring the nature of chlorine emissions. Sea-salt particle source functions are evaluated in order to select appropriate representations of sea-salt particle generation. The

compilation of a detailed gas-phase chlorine chemistry mechanism is presented followed by a description of the treatment of heterogeneous/multiphase chemical reactions in the model. Model simulations are performed and compared to a base case scenario where sea-salt reactions are excluded. Finally, additional simulations explore the effect of other unknown reactions or sources of chlorine may have on urban ozone dynamics. Suggestions for further experimental, modeling and field studies are also provided.

1.2 Chlorine Emissions and the Model Domain

Chlorine compounds found in the troposphere are divided into two main categories according to organicity. The Reactive Chlorine Emissions Inventory (RCEI) campaign has produced a global emissions inventory of reactive chlorine species (defined as those species with a lifetime less than 10 years) [*Khalil et al.,* 1999; *Erickson et al,* 1999; *Keene et al.,* 1999]. According to the study, most of the chlorine atoms in the troposphere are bound to carbon atoms. With the exception of chloroform, global emissions of halocarbon molecules are dominated by anthropogenic activities. However, inclusion of organochlorine species into an urban photochemical airshed model is not necessary at the present time. The impact of these species as volatile organic compounds on urban ozone formation is negligible due to their extended lifetimes and low ambient concentrations (see Table 1).[†] Although halocarbons are important when analyzing the chemistry of the total global atmosphere, the current study is limited to the study of the effect inorganic chlorine species on the chemistry leading to ozone formation within the lower troposphere of urban coastal regions.

The vast majority of the inorganic chlorine in the troposphere is found as chloride contained in sea-salt aerosol generated from ocean-wind and ocean-surf interactions [*Gong et al.,* 1997b; *Erickson et al.,* 1999; *Keene et al.,* 1999]. There are few other natural sources of inorganic chlorine, with notable exceptions including particulate chloride contained in wind blown soils, particularly in arid and semi-arid regions, and hydrochloric acid emissions from active volcanoes. Anthropogenic sources of inorganic

[†] However, due to their toxicity even at low concentrations, many organochlorine species are presently controlled by the ARB and form part of the board's Toxic Emissions Inventory, e.g. $CHCl_3$, CH_2Cl_2, C_2Cl_4 and C_2HCl_3.

chlorine explored by the RCEI include coal combustion, biomass burning (90% generated from human activities) and waste incineration. The principal chlorine-containing byproduct of these activities is hydrochloric acid and, in the case of biomass burning, particulate chloride. A segment of reactive chlorine emissions not considered by the RCEI is direct emissions of Cl_2 from industrial plants. For instance, a site near Salt Lake City, Utah reported emissions of 44,300 tons/yr (0.0443 Tg/yr) of Cl_2 in 1988 [*Reynolds,* 2001]. More recently, it has been estimated that emissions of Cl_2 within Harris County, Texas, (the principal country of the Houston metropolitan area) averaged ~172,000 pounds per year in the period from 1998-1999 [*Harris County, Texas, Pollution Control Division,* 2001].

Table 1: Distribution of reactive chlorine species in the troposphere

Species		Source	% of tropospheric reactive chlorine*	Globally averaged concentration*	Approximate lifetime τ_{OH} **
CH_3Cl	methyl chloride (chloromethane)	Anthropogenic and natural	43%	540 ppt	~10 months
CH_3CCl_3	methyl chloroform (1,1,1 trichloroethane)	Mainly Anthropogenic	29%	120 ppt	~ 3 years
$CHCl_3$	chloroform (trichloromethane)	Mostly natural	4%	16 ppt	~ 4 months
CH_2Cl_2	methylene chloride (dichloromethane)	Mainly anthropogenic	3%	18 ppt	~ 2 months
C_2Cl_4	Perchloroethylene (Tetrachloroethene)	Mostly anthropogenic	2%	6 ppt	~ 3 months
Other organo-chlorine species			11%		
Sum of % total reactive chlorine			93%		

* [*Khalil et al.,* 1999]
** $\tau_{OH:}$ Lifetime with respect to a typical average [OH] = 1×10^6 molecule cm^{-3} at 298 K and 1 atm.

The terrain of the South Coast Air Basin of California (SoCAB) is characterized by extensive urban development delimited by the forest regions to the north and east (see Figure 1). The SoCAB is devoid of any volcanic activity. The small semi-arid region in the northwest section of the domain is unlikely to influence atmospheric chlorine loads significantly compared to the nearby coast. In addition, the semi-arid regions in the eastern section of the domain are too far downwind to impact the chemistry of the overall basin. Coal combustion and biomass burning are not heavily practiced in the South Coast Air Basin of California; electricity generated within the basin is generated primarily by oil/gas-fired and

hydroelectric power plants [*California Energy Commission,* 2001]. Although a few municipal solid waste incinerators are scattered within the airshed, it is unknown how much hydrochloric acid escapes from these facilities. Given these characteristics of the domain and the lack of information on chlorine emissions from sources such as industrial activity and swimming pools, this research shall focus on the determination and quantification of the effect of chlorine originating from the Pacific Ocean on the air quality of the Greater Los Angeles Metropolitan Area. Nonetheless, further simulations are performed in order to infer the effect of additional sources of chlorine on the dynamics of ozone formation.

Figure 2: Computational domain of CIT Airshed Model (994/1150 cells within a 115 × 250 km subset of the master domain). Yellow, light blue and dark blue cells represent land, surf and open-ocean regions. Grey circles represent monitoring stations. The violet "strip" denotes a region used to show "slices" of contour plots.

2. Materials and Methods

2.1 Host Model and Principal Assumptions

The host model used for the current study is based on the Caltech (CIT) Airshed Model. This parallel-code version of the model is under continuous development at the University of California, Irvine in collaboration with researchers from the California Institute of Technology and other institutions [*McRae et al*., 1982; *McRae and Seinfeld*, 1983; *Harley et al*., 1993; *Meng et al*., 1997, 1998; *Griffin et al*., 2002b]. In application to the SoCAB, the horizontal domain of the model is an 80 by 30 grid with a resolution of 5 km; vertical resolution consists of five layers up to 1100 m above the surface. A computational domain consisting of 994 five-cell columns is derived from an 1150-column (115 km × 250 km) subset of the master domain is used for this study (Figure 2). The computational domain encompasses the major ocean, surf, urban and rural regions that influence the air quality of the South Coast Air Basin of California and contains over 90% of the population of the master domain.

The model employs the new CACM chemical mechanism, consisting of 361 chemical reactions, and tracks 123 gas-phase species. The CACM mechanism is based on the SAPRC-97 [*Carter et al.,* 1997a], RACM [*Stockwell et al.,* 1997] and MCM [*Jenkin et al.,* 1997] chemical mechanisms. The gas-phase chemistry mechanism has been validated successfully by evaluating its performance in simulating the August 27-29 SCAQS episode [*Griffin et al.,* 2002a].

Dynamic aerosol computations simulate the fate of 37 inorganic and organic aerosol species over 8 size bins, characterized by mass, ranging from 0.039 to 10 micrometers in diameter. The thermodynamics module Simulating Composition of Atmospheric Particles at Equilibrium 2 (SCAPE2) is used to describe the gas-aerosol partitioning of inorganic aerosol constituents [*Kim et al.,* 1993; *Meng et al*., 1995]. The CACM mechanism includes detailed treatment of secondary VOC (SVOC) formation. Partitioning of secondary organic oxidation products to either an aqueous or an absorptive organic aerosol phase is determined using a new thermodynamic module coupled to SCAPE2 [*Pun et al.*, 2002]. The current version of the CIT Airshed Model and its performance in simulating the formation and fate of SOA in the SoCAB is described in full by *Griffin et al.,* [2002b].

The UC Irvine/Caltech Airshed Model is a powerful tool for assessing the influence of sea-salt on the South Coast Air Basin of California. However, there are important assumptions and limitations which may be relaxed in the future as part of a more comprehensive research project. First, aerosol particles are modeled using an internally mixed assumption, i.e. all particles within a size bin are assumed to have the same composition. This assumption provides adequate results, particularly when comparing measurements of 24-hour averaged concentration of aerosol constituents with model predictions. However, improved results may be obtained by simulating a source-based external mixture. Initially, two general categories may be considered, marine origin and urban/terrestrial origin, to better determine the effect of sea-salt aerosol on urban air quality.

Second, apart from several equilibrium expressions, aqueous-phase chemical reactions are absent from the computations. Heterogeneous/multiphase chemistry is treated excluding reactions occurring in the bulk of the aqueous component of atmospheric aerosol particles. The reactions considered in this study are believed to represent key processes leading to reactive chlorine concentrations in urban coastal regions. However, a definitive study must consider the effect of aqueous-phase chemistry within coastal aerosol. The composition and water content of urban aerosol may initially limit aqueous-phase chemistry modeling to the marine-origin aerosol. Indeed, current photochemical models that include aqueous-phase reactions limit the scope of their studies to marine boundary layer and cloud simulations [*Sander and Crutzen,* 1996; *Vogt et al.,* 1996; *Hermann et al.,* 2000; *Moldanova and Ljungstrom,* 2001; *Toyota et al.,* 2001]. Thus, incorporation of aqueous-phase chemistry should be considered only after the source-based external mixture approximation is implemented. The model currently requires 16 hours to simulate a two-day episode on a 64 node parallel computer. Simulation of an external mixture and incorporation aqueous-phase chemical reactions would require a vast amount of computer resources.

The three principal components added to model – the sea-salt aerosol source functions, the gas-phase chlorine chemistry mechanism, and the treatment of heterogeneous/multiphase chemical reactions – are described in the following sections. This section concludes with discussions on the preparation of meteorological and emissions data for the air quality episode selected for this study.

2.2 Sea-salt Particle Source Functions

Accurate sea-salt aerosol flux expressions are necessary to determine adequately the amount of chlorine-containing gases released from these particles. Sea-salt aerosol in the size range pertinent to air quality studies is produced primarily from the bursting of air entrained bubbles from oceanic whitecaps [*Woolf et al.,* 1987; *Fitzgerald,* 1991; *Wu,* 1994; *Spiel*, 1994a, 1994b, 1995, 1997, 1998]. This phenomenon has been studied extensively in order to determine sea-salt aerosol fluxes as a function of wind speed as part of investigations of moisture and heat fluxes at the ocean-air interface and atmospheric processes [*Andreas,* 1990, 1992, 1998; *Stramska et al.*, 1990; *O'Dowd et al.,* 1993; *Smith et al.,* 1993; *Edson and Fairall.,* 1994; *Andreas et al.,* 1995, 2001; *DeCosmo et al.,* 1996; *Pattison and Belcher,* 1999; *Reid et al.,* 1999].

Open ocean whitecaps develop primarily due to the breaking of wind-induced waves. Open ocean aerosol fluxes are calculated using the function of Monahan and coworkers [*Monahan et al.,* 1986] widely used in global atmospheric sea-salt aerosol models [*Gong et al.,* 1997a; *Erickson et al,* 1999]

$$\frac{dF_{N-Open}}{dr_{80}} = 1.373 \times U_{10}^{3.41} \times r_{80}^{-3} \times (1 + 0.057 r_{80}^{1.05}) \times 10^{1.19 e^{-B^2}} \qquad (1)$$

where $B = (0.380 - \log r_{80})/0.650$. In the preceding equation, dF_{N-Open}/dr_{80} represents the number of particles generated per unit area of ocean/sea surface per second per unit increment in droplet radius at a reference relative humidity of 80%, r_{80}. The corresponding units of Equation 1 are particles m^{-2} s^{-1} μm^{-1}. U_{10} is the wind speed, in m/s, at an elevation of ten meters from the water surface. This open ocean source function applies to particles with radii at 80% RH between 0.8 μm and 10 μm.

The investigation of the generation of aerosol in the surf zone, where sea-salt aerosol concentrations have been measured 1–2 orders higher than the oceanic background, is on the forefront of ocean-atmosphere research [*De Leeuw et al.,* 2000]. In this littoral region, wave breaking is dominated by interaction with the sea bottom surface. Extensive, near complete, whitecap coverage can therefore develop even at very low wind speeds. The extent of bubble-mediated aerosol production is determined by the energy dissipated by the breaking waves and is therefore also dependent on wind speed. *De Leeuw*

et al. [2000] recently investigated surf-zone particle generation off the California coast, thus generating a wind-speed dependent mathematical expression suitable for simulating the flux of sea-salt aerosol to the coastal boundary layer,

$$\frac{dF_{N-Surf}}{dD_0} = 1.1\times10^7 \times e^{0.23\times U_{10}} \times D_0^{-1.65}. \quad (2)$$

In the preceding equation, dF_{N-Surf}/dD_0 represents the number of particles generated per unit area of ocean/sea surface per second per unit increment in droplet diameter at formation, D_0. The units of Equation 2 are also particles m^{-2} s^{-1} μm^{-1}. This surf zone source function applies is applicable up to wind speeds of 9 m/s and for particles with diameters at formation between 1.6 μm and 20 μm. This source function reproduces significant sea-spray particle concentrations that are present in the littoral zone at very low, even null, wind speeds. Models of coastal aerosol transport have shown that the production of surf-zone generated particles cannot be ignored and must be accounted for in photochemical models that include heterogeneous/multiphase reactions on sea-salt aerosol [*Vignati et al.,* 2001].

The previous sea-salt particle flux approximations exhibit no dependency on other meteorological parameters such as temperature or relative humidity. Nonetheless, *Stramska et al.* [1990] have performed experiments that suggest that production of bubble-mediated aerosol may be enhanced in supersaturated seawater. The extent of saturation of the main atmospheric gases, nitrogen and oxygen, in water is dependent on both water and air temperature; biological activity off the California coast can also result in dissolved oxygen supersaturation by as much as 85% [*Stramska et al.,* 1990]. As expressed earlier, surf-zone generated sea-salt aerosol is also highly dependent on the sea bottom topography. For the purposes of this study, where surf-zone production dominates sea-salt particle mass loadings, both the California-coast derived expression of *DeLeeuw et al.* [2000] and the open-ocean expression of *Monaham et al.* [1986] are considered adequate.

There are several different conventions for representing sea-salt aerosol production rates. In this case, the open ocean function is given in terms of the particle radius at a reference relative humidity of 80% (r_{80}) and the surf-zone density function is respect to the actual diameter at formation (D_0). A brief

discussion on the fate of fresh sea-salt particles is presented in order to determine which representation is more amenable to the CIT Airshed Model.

Upon ejection, sea-salt particles have a composition similar to that of seawater. The droplets then come to the equilibrium with the ambient relative humidity at the ambient temperature. In the CIT Airshed Model, evaporation and condensation of water from and to all aerosol particles is treated by the SCAPE2 thermodynamic module accounting for relative humidity and temperature. The water content of the particles is estimated using the Zdanovskii-Stokes-Robinson (ZSR) relation [*Robinson and Stokes*, 1965] as a fundamental part of the module. Given this treatment of aerosol particles in the model, it is preferable to generate particles in their natural form and allow the model to establish their fate. Using the relations [*Andreas*, 1998; *Andreas et al.,* 2001]:

$$\frac{dr_{80}}{dr_0} = 0.506 r_0^{-0.024} \text{ and } \frac{dr_0}{dD_0} = \frac{1}{2}, \tag{3, 4}$$

where r_0 is the radius at formation, the open ocean source function is expressed now by

$$\frac{dF_{N-Open}}{dD_0} = \frac{dF_{N-Open}}{dr_{80}} \frac{dr_{80}}{dr_0} \frac{dr_0}{dD_0}. \tag{5}$$

The particle number and mass flux resulting from the source functions are compared in Figure 3 for a wind velocity of 2 m/s. The open-ocean and surf-zone source functions incorporated into the airshed model simulate sea-salt aerosol production in a surf zone span of ~ 230 km and an open-ocean region of ~3850 km^2 within the computational domain. The width of the surf-zone was estimated at 100 m. This value is on the higher end of observed values by *De Leeuw et al.* [2001]. However, this width was chosen to account roughly for the fraction of particles formed beyond the upper limit of the aerosol diameter range in the model (10μm) that are expected to decrease in size upon reaching equilibrium with the ambient relative humidity.

It is expected that fresh sea-salt aerosol concentrations near the surf zone will be somewhat high. This should not pose any health concerns, as fresh sea-salt particles are rather benign. Fresh sea-salt aerosol have a composition similar to human plasma (see Table 2) and NaCl is commonly used as a harmless

sham control that is injected into the lungs of rats in aerosol exposure studies [*K. Berube*, personal communication]. Although larger sea-salt particles will deposit or settle quickly, the smaller particles can provide surfaces for soluble ionic species that may cause damage to the lungs, e.g. PAHs, to condense. The urban processing of sea-salt aerosol is therefore of concern, but beyond the scope the current study.

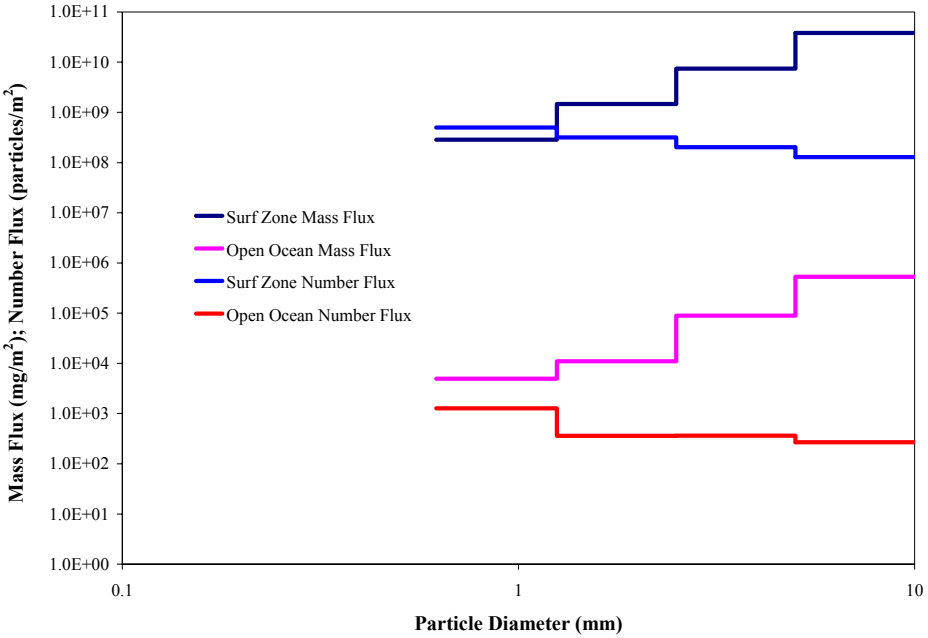

Figure 3: Comparison of sea-spray source functions: Flux of sea-salt particles at 2 m/s wind velocity

Table 2: Typical composition of seawater

Species	**Conc. mg/kg**	**Mass fraction**	**Molecular weight**
Cl^-	19352.9	55.02%	35.45
Na^+	10783.8	30.66%	22.99
SO_4^{2-}	2712.4	7.71%	128.13
Mg^{2+}	1283.7	3.65%	24.31
Ca^{2+}	412.1	1.17%	40.08
K^+	399.1	1.13%	39.10
HCO_3^-	107.0	0.30%	61.02
Br^-	67.2	0.19%	79.90
$B(OH)_3$	19.4	0.06%	61.83
CO_3^{2-}	16.1	0.05%	60.01
Sr^{2+}	7.9	0.02%	87.62
F^-	6.8	0.02%	19.00
Other	3.6		
Total	**35172.0**		

[*Millero*, 1996]

2.3 Gas-Phase Chlorine Chemistry Mechanism

Twelve gas-phase species and 83 gas-phase reactions have been added to the host model in order to represent the chemistry of photochemically active chlorine-containing gases derived from sea-salt particles. The rate constant of these reactions reflect the most recent recommendations from IUPAC [*Atkinson et al.*, 1997a, 1997b, 1999, 2000] and NASA/JPL [*DeMore et al.*, 1997; *Sander et al.*, 2000] evaluations. These values were corroborated and updated with the latest published results of oxidation of VOC by chlorine atoms in the atmosphere [*Atkinson*, 1997; *Pilgrim et al.*, 1997; *Stutz et al.,* 1998; *Coquet and Ariya*, 2000; *Notario et al*., 2000a, 2000b]. The products of the oxidation of isoprene by Cl atoms were assumed reflecting the best knowledge of the mechanism [*Ragains and Finlayson-Pitts*, 1997; *Notario et al.*, 1997; *Fantechi et al.*, 1998; *Finlayson-Pitts et al.,* 1999; *Canosa-Mas et al.,* 1999; *Suh and Zhang,* 2000]. A full listing of the gas-phase chlorine chemistry reaction mechanism is given in Appendix A at the end of this report.

The gas-phase chlorine chemistry mechanism in this study represents the most detailed compilation of its kind ever implemented into an urban photochemical model. In contrast, the chlorine chemistry mechanism developed for simulation of the Houston area [*Tanaka and Allen*, 2001] includes only 13 reactions: the photolysis of Cl_2 and HOCl, 3 inorganic reactions, and 8 organic reactions (see Table 3). The mechanism of *Tanaka and Allen* was developed for use with the Carbon Bond IV Mechanism and is limited to the oxidation of methane, lumped $\geq C_2$ alkanes, ethene, lumped $\geq C_3$ alkenes, isoprene and 1-3 butadiene. It must be noted that the mechanism of Tanaka and Allen is concise by design and that it has produced important findings as discussed later in this manuscript. Although a succinct mechanism may be favorable in certain scenarios, this study opts for the other end of the spectrum: comprehensiveness.

There are limited chamber data at present to test chlorine radical initiated VOC oxidation mechanisms [*California Air Resources Board*, 1999]. Consequently, significant uncertainties arise during mechanism development. First, Cl radical VOC oxidation reactions that proceed by addition to carbon double bonds produce organic intermediate products for which the rate constants of ensuing reactions are not well known. (Conveniently, Cl radical initiated VOC oxidation reactions that proceed by hydrogen

abstraction, forming HCl, generate intermediate products identical to the analogous reaction initiated by OH to form H_2O.) Several complex reaction mechanisms, such as that of the chlorine initiated oxidation of isoprene, are still not well characterized. Finally, the selection of rate constants for lumped organic (intermediate and non-intermediate) species has not undergone rigorous validation by chamber experiments.

An attempt has been made to reduce the uncertainties by including as much detail as possible and incorporating the chlorine chemical mechanism to a host photochemical model already possessing a high degree of VOC speciation [*Griffin et al.,* 2002a]. The reactions of several chlorine-containing organic intermediate products are included, in addition to the reaction of the Cl radical with other organic radical intermediates (see Table 3). The mechanism presented here is an initial step in the development of a comprehensive chlorine chemistry mechanism for urban photochemical modeling. Nonetheless, for the purpose of this study, the mechanism is more than satisfactory to provide a first estimate of the impact of sea-salt derived chlorine chemistry in urban coastal regions.

Table 3: Comparison of different mechanisms of chlorine chemistry used in modeling of urban air quality

Report	*Tanaka and Allen*, 2001	This work
Host chemical mechanism	Carbon Bond IV (CB–IV)	CalTech Chemical Mechanism (CACM)
Host photochemical model	CAMx [*Chang et al.*, 2002]	CIT Airshed Model
Photolysis reactions	2 – Cl_2, HOCl	8 – Cl_2, HOCl, ClNO, $ClNO_2$, $ClONO_2$, OClO, ClONO, HCOCl
Inorganic reactions	3	35
Oxidation of organics by the Cl radical	6 – methane, ≥ C_2 alkanes, ethene, ≥ C_3 alkenes, isoprene and 1-3 butadiene	14 – methane, C_2–C_6 alkanes, C_7–C_{12} alkanes, > C_{12} alkanes, ethene, C_3–C_6 alkenes, > C_6 alkenes, methanol, ethanol, ≥ C_2 alcohols, MTBE, C_3–C_6 ketones, > C_6 ketones, isoprene
Intermediate organic reactions	2	26
Total reactions	13	83

2.4 Heterogeneous/Multiphase Chemical Reactions

The distinction between heterogeneous and multiphase reactions in the field of atmospheric sciences is quite subtle. *Ravishankara* [1997] presents a brief review of heterogeneous and multiphase reactions, offering a distinction between the two terms. Heterogeneous reactions are defined as reactions occurring between gases on the surface of solids, or on a quasi-liquid layer above a solid. Multiphase reactions are defined as the transfer into a condensed phase of gas-phase species followed by reaction entirely in the bulk of the condensed phase (solution-phase or aqueous-phase). The products of a multiphase reaction may remain in the condensed phase or diffuse and transfer back to the gas phase. The findings of *Knipping et al*., [2000] suggest that further distinction must be made when referring to heterogeneous reactions in order to include reactions occurring at the gas-liquid interface of atmospheric particles. Following is a modified version of the distinction provided by *Ravishankara* [1997] taking this aspect into consideration:

- Heterogeneous reaction on solids: The reaction is confined to the quasi-liquid layer (if present) of a solid or on the surface of liquid. Diffusion into and out of the bulk of the solid is assumed to be too slow to affect concentrations at the surface. Products are released to the gas and formed on the solid phase.
- Heterogeneous (interfacial) reaction on liquids: The reaction is confined to the surface or gas-liquid interface of a liquid. Diffusion into and out of the bulk of the liquid is assumed to be slow or otherwise hindered and a mechanism exists for surface replenishment of the reacted species. The surface replenishment process does not necessarily restore surface concentrations to their original value. Products may remain at the interface or partition between the gas or condensed phase depending on solubility.
- Multiphase reaction: The reaction takes place once the molecule has crossed the air-liquid interface and has been incorporated into the bulk of the condensed. The products of a multiphase reaction may remain in the condensed phase or diffuse and transfer back to the gas-phase.

If follows that reactions occurring entirely in a condensed phase that do not involve species previously transferred from the gas-phase – regardless of whether the products of these reactions eventually transfer into the gas phase due to solubility limitations – should be referred to as simply solution-phase reactions, or aqueous-phase reactions when water is the principal solvent. However, the more common practice in atmospheric modeling is to refer to multiphase and solution-phase (or aqueous-phase) modeling together as a single concept. Thus, any future reference made to modeling of an aqueous phase shall refer to both aqueous-phase and multiphase modeling unless an explicit distinction is made.

There are several models of marine boundary layer processes that include aqueous-phase modeling, including MOCCA [*Sander and Crutzen*, 1996] and CAPRAM [*Hermann et al.*, 2000]. However, the computational resources required to depict accurately the aqueous-phase component of marine aerosol in an urban airshed are prohibitive at the moment. As discussed in the introduction, the internally-mixed assumption must be relaxed first. In addition, a complete aqueous-phase chemical system coupled to the gas phase would require simultaneous solution across all marine-aerosol size bins. Computation of aerosol thermodynamics for non-marine aerosols would also be required. Although high performance computing resources continue advancing at a rate that solution of this complex system could become feasible before long, incorporation of a full aqueous-phase treatment into an externally-mixed aerosol model is clearly beyond the scope of the current study.

A description of the heterogeneous/multiphase chemistry included in this study and their treatment in the CIT Airshed Model is given on the following pages.

A series of experiments, in combination with theoretical and numerical modeling, provide strong evidence in support of a mechanism of chlorine formation initiated by the heterogeneous reaction of the hydroxyl radical with chloride ions at the gas-liquid interface of deliquesced salt particles [*Oum et al.,* 1998; *Knipping et al.*, 2000].

$$OH_{(gas)} + Cl^-_{(aerosol)} \rightarrow \tfrac{1}{2}\, Cl_{2(gas)} + OH^-_{(aerosol)} \qquad (6)$$

Knipping and Dabdub [2002] have determined that an overall expression for this rate of this reaction, R_6, can be approximated using a simple collision uptake expression,

$$R_6 = \frac{1}{2}\frac{d[\mathrm{Cl}_2]}{dt} = \gamma_s \frac{\omega}{4} A[\mathrm{OH}] \quad (7)$$

where ω is the mean molecular speed of an OH particle, A is the particle surface area, and γ_s is the reactive uptake coefficient given by

$$\gamma_s = 0.04[\mathrm{Cl}^-] \quad (8)$$

where the constant (0.04) has units of M^{-1}. A $[\mathrm{Cl}^-]$ dependency in γ_s is a necessary element in order to enhance the reaction as the particles become more concentrated and to quench the reaction as the particles become depleted in chloride. In general, the reactive uptake coefficient can be decomposed into various physicochemical parameters that take into account potential limitations due to gas-phase diffusion, mass accommodation to a condensed-phase, condensed-phase diffusion, and chemical reaction [*Hanson*, 1997; *Finlayson-Pitts and Pitts*, 2000]. Due to the uncertainties in the system, the determination of γ_s was narrowed to the compact expression given by Equation 8.

The multiphase reactions of dinitrogen pentoxide (N_2O_5) [*Fenter et al.,* 1996; *Behnke et al.*, 1997; *Schweitzer et al.,* 1998; *Gebel and Finlayson-Pitts,* 2001], and chlorine nitrate ($ClONO_2$) [*Caloz et al.,* 1996; *Wincel et al.,* 1997] with sea-salt particles are also included in the model mechanism:

$$N_2O_{5(gas)} + Cl^-_{(aerosol)} \rightarrow ClNO_{2(gas)} + NO_3^-{}_{(aerosol)} \quad (9)$$

$$ClONO_{2(gas)} + Cl^-_{(aerosol)} \rightarrow Cl_{2(gas)} + NO_3^-{}_{(aerosol)} \quad (10)$$

These reactions also release chlorine into the atmosphere in forms that photolyze and generate chlorine atoms. Aqueous-phase models [*Sander and Crutzen*, 1996; *Moldanova and Ljungstrom*, 2001] simulate these reactions by transferring the species into the aqueous-phase of sea-salt particles using the mass-transfer method of *Schwartz* [1986]. Upon entering the aqueous-phase, the species are assumed to hydrolyze, react with chloride or react with bromide. The partitioning of these reactions is handled by a method developed by *Behnke et al.* [1994, 1997]. Other models, in particular stratospheric models, use complex phenomenological uptake models to determine the uptake coefficient of reactions similar to Reactions 9 and 10 [*Hanson et al*., 1994; *Donaldson et al*., 1997; *Robinson et al*., 1997].

Although JPL & IUPAC recommendations were considered for the modeling of Reactions 9 and 10 using phenomenological uptake models [*DeMore et al.*, 1997; *Sander et al.*, 2000; *IUPAC,* 2000], results from uptake studies on solid salts, salt powders and fresh synthetic sea-salt aerosol are not readily transferable to urban airshed models. The method employed by the marine boundary layer models appears promising once a full aqueous-phase and external mixture is developed into the model. Given the current limitations and the scope of this study, the rate of Reactions 9–10 was approximated using an expression analogous to Equation 7 but with $\gamma_s = 0.02[Cl^-]$.

The reaction of the nitrate radical on sea-salt particles,

$$NO_{3(gas)} + Cl^-_{(aerosol)} \rightarrow \tfrac{1}{2}\, Cl_{2(gas)} + NO_3^-{}_{(aerosol)} \qquad (11)$$

is added to the other reactions in a second simulation in order to gain insight on the effect of a potential nighttime mechanism for chlorine release from sea-salt particles. The possibility of this reaction occurring, and the extent to which it may occur, is uncertain. However, this simulation provides a sensitivity analysis of the impact of nighttime halogen accumulation in a coastal region. This reaction is modeled in a fashion similar to Reactions 9 and 10.

Included in the SCAPE2 thermodynamic module [*Kim et al.,* 1993*; Meng and Seinfeld,* 1995] of the CIT Airshed Model are several heterogeneous/multiphase equilibrium reactions that account for HCl displacement by less-volatile stronger acids, such as nitric and sulfuric acid. These reactions may be summarized as follows,

$$HNO_{3\,(gas)} + XCl_{\,(aerosol)} \leftrightharpoons HCl_{\,(gas)} + XNO_{3\,(aerosol)} \qquad (12)$$

$$H_2SO_{4\,(gas)} + 2\ XCl_{\,(aerosol)} \leftrightharpoons 2\ HCl_{\,(gas)} + X_2SO_{4\,(aerosol)} \qquad (13)$$

$$H_2SO_{4\,(gas)} + XCl_{\,(aerosol)} \leftrightharpoons HCl_{\,(gas)} + XHSO_{4\,(aerosol)} \qquad (14)$$

where X denotes a cation such as Na^+, NH_4^+, K^+ or H^+. Other equilibrium reactions are included in the SCAPE2 module that form diprotic salts (involving Mg^{2+} and Ca^{2+}), in addition to further reactions that form carbonate and bicarbonate salts. The salts consumed and/or formed in Reactions 12–14 can be either in dissolved or solid form, depending on the overall thermodynamics of the system as dictated by the

particle composition, water activity (relative humidity) and temperature. The reaction of hydrochloric acid with the hydroxyl radical in the gas phase,

$$HCl + OH \rightarrow Cl + H_2O, \quad (15)$$

is relatively slow. Therefore, although most of the chloride is expected to exit the sea-salt particles as HCl by Reactions 12–14, it is Reactions 6 and 9–11 that are expected to dictate chlorine radical concentrations in the model due to their highly photolyzable gaseous products.

2.5 Meteorology

Air quality simulations of conditions of September 8 – 9, 1993 are presented in this study. During this period, particularly high 1-hour average ozone concentrations were recorded for the South Coast Air Basin of California. A high pressure system developed over the air basin and a strong temperature inversion aloft limited vertical mixing. Conditions were quite sunny and hot, with peak temperatures in the eastern region of domain exceeding 40 ºC, leading to enhanced photo-oxidation rates.

Meteorological data for this episode were supplied by the South Coast Air Quality Management District (SCAQMD). These parameters include relative humidity, temperature, wind, ultraviolet solar radiation, total solar radiation, and mixing height. A description of how the meteorological parameters were prepared is given by *Griffin et al.,* [2002b]:

> Meteorological parameters were obtained from a variety of sources. Hourly observations of surface wind speed and direction were taken at 21 sites by the California Irrigation Management Information Service (CIMIS) and at 32 sites by the SCAQMD. Temperature and relative humidity data were recorded at the 21 CIMIS sites, at 13 of the SCAQMD sites, and at 52 sites operated by the National Climatic Data Center. Total solar radiation was monitored by SCAQMD at six sites and by CIMIS at its 21 sites. Ultraviolet radiation was measured at one site in Central Los Angeles by SCAQMD. Hourly gridded fields for these types of data were made using the methodology described in *Harley et al*. [1993]. Inversion base height and wind aloft were inferred from upper air measurements made daily by SCAQMD in West Los Angeles at 0500 PST and by CARB in Claremont between 0600 and 1400 PST. *Winner and Cass* [1999] demonstrate the method used for creating mixing depth fields from such data.

Temperature affects the kinetics of gas-phase reactions, as well as the equilibrium constants and deliquescence points of the mixed inorganic salts modeled by the SCAPE2 module. Relative humidity and temperature are used to determine the amount of gas-phase H_2O present, which can participate in a number of reactions, including the reaction with $O(^1D)$ to form the hydroxyl radical. Relative humidity also determines the amount of water that partitions between the gas phase and aerosol phase, thus determining the salt concentration of freshly formed sea-salt particles reach upon reaching equilibrium.

2.6 Emissions

Gas and particulate emissions inventory for this episode were supplied directly by the South Coast Air Quality Management District, except for sea-salt particle emissions that were calculated using either the open ocean or surf-zone sea-salt particle source functions described earlier in Section 2.2. A description of how the gas-phase emissions were prepared is given by *Griffin et al.,* [2002b]:

> Hourly gas-phase emissions (point and mobile sources) for each of the model grid cells were supplied by SCAQMD. The baseline emissions inventories used for the modeling exercise were generated by the SCAQMD for 1993 as a part of the 1997 Air Quality Management Plan. The emissions inventories reflect both collected available information and projections for the automobile fleet and industrial emissions of 1993. The biogenics emissions inventory was represented using the biogenics emissions inventory developed for the late August episode of the SCAQS. It is assumed that the amount and type of vegetation located in the SoCAB in the late summer and early fall likely did not change significantly between 1987 and 1993. Mobile source emissions were generated through use of the California Air Resources Board (CARB) emissions model EMFAC-7G [*California Air Resources Board*, 1998]. Gas-phase emissions are broken down into ammonia, oxides of sulfur (SO_x), oxides of nitrogen (NOx), CO, and organic species. … Organic species are lumped according to chemical structure and functionality, and experimentally determined SOA forming potential. … If only total organic emissions are known for a given source, the split among the groups is assumed based on the observed ambient data. These splits are also used to establish boundary and initial conditions … Previous work has shown that on-road motor vehicle emissions in the SoCAB have been under-predicted significantly by the methodology used to develop spatially and temporally resolved emission patterns from SCAQMD emission inventories [*Pierson et al.*, 1990; *Fraser et al.,* 1998]. Therefore, hot exhaust emissions of volatile organics and CO from light duty vehicles were increased by a factor of 3 (see, for

example, *Harley et al.* [1993] and *Fraser et al.* [2000]). Ammonia emissions are based upon the inventory of *Gharib and Cass* [1984].

Hourly aerosol-phase emissions are apportioned into eight size sections, and the appropriate mass of each species is placed into the proper size bin at the corresponding cell [*Fraser et al*., 2000]. Aerosol species include sodium, chloride, ammonium, sulfate, nitrate, calcium, magnesium, and potassium, elemental carbon, organics, and unidentified/other material. Initial and boundary conditions for PM are based on observed aerosol distributions obtained during the SCAQS sampling campaign [*John et al*., 1990].

3. Results

3.1 'Base Case' simulation

In order to evaluate the effect of sea-salt derived chlorine chemistry, a "Base Case" simulation must be performed. These model results serve as a gauge of the performance of the model without the newly added chemical reactions, i.e. the complete gas-phase chlorine chemistry mechanism and four of the heterogeneous/multiphase reactions (6 & 9–11). The equilibrium reactions (12–14) treated by the SCAPE2 thermodynamic module are included in these simulations in order to account for chloride depletion due to HCl displacement by less-volatile stronger acids. These results provide a benchmark for comparison of different simulation scenarios. The newly incorporated sea-salt particle source functions are also included in the Base Case simulation; however, an evaluation of these functions is delayed until the subsequent section. Results for the second day of the Base Case simulation are presented in Figure 4.

Figure 4 illustrates how ozone concentrations increase throughout the eastern region of the domain as the day progresses. The ozone contour plots also manifest the complexity of the air quality episode selected for this study. The low ozone concentrations in the center region of the domain are attributed to NO_x titration of ozone by the model. Investigations are underway on the potential for ozone formation due to renoxification of the atmosphere in collaboration with the Finlayson-Pitts research group at the University of California, Irvine, in order to better reproduce ozone concentrations in this region.

The eastern boundary of the domain retains high ozone concentrations during the night. These high concentrations are caused by two factors. First, there exist inherent difficulties that numerical models encounter when simulating meteorological conditions at the mountainous boundary of the computational domain. Wind patterns develop in the vicinity of the Banning pass and extend northeast into San Bernardino Mountains that are difficult for the model to resolve, particularly at boundaries. Air parcels drift up and effectively undergo recirculation towards the west in the upper levels, thus rebounding ozone back into the model.

Second, *Griffin et al.,* [2002b] have determined that the conventional method used to calculate vertical eddy diffusivities in the CIT Airshed Model under-predicts these parameters at the low wind

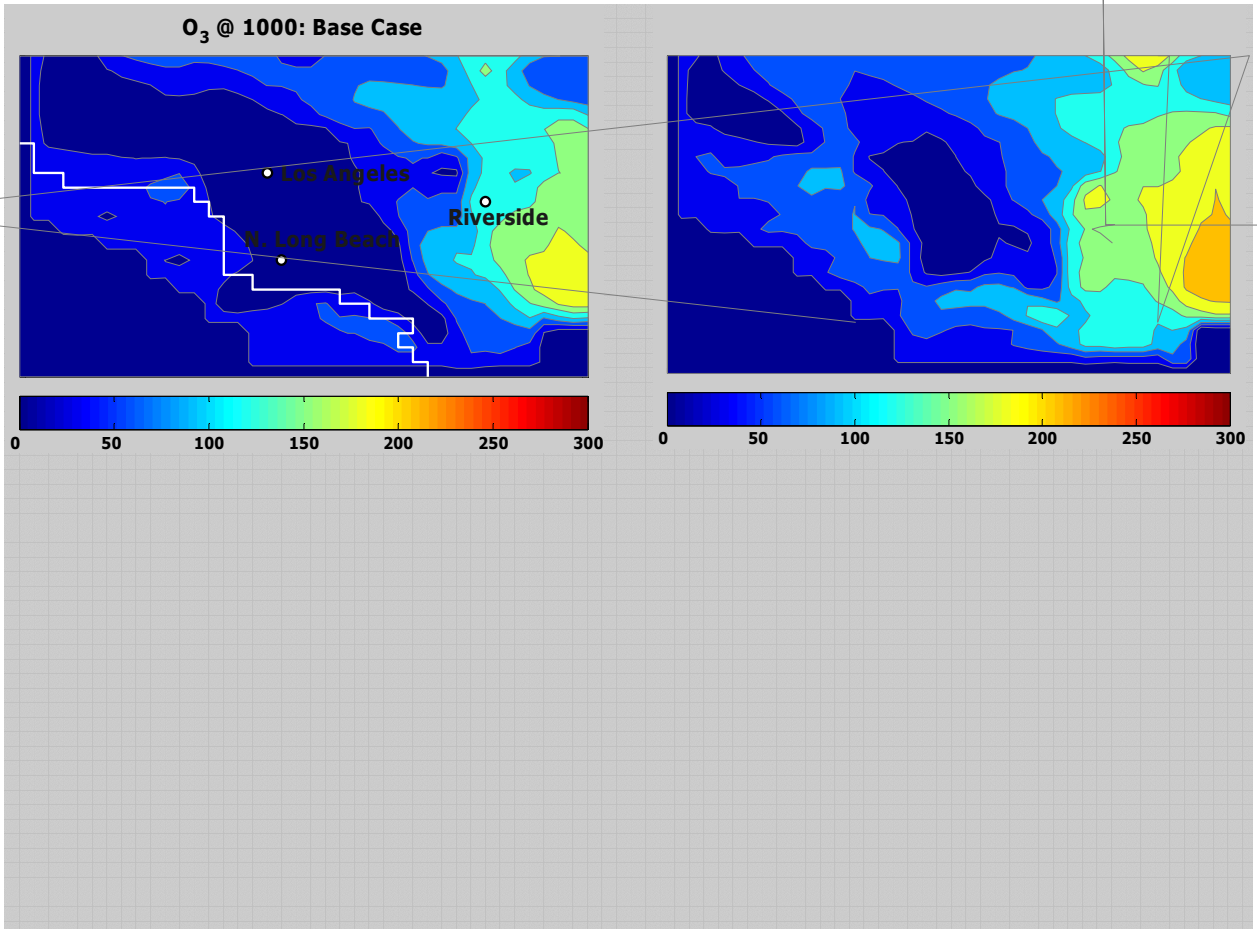

Figure 4: Ozone concentration contours – Base Case simulation: September 9, 1993 (all units in ppb). Results are shown at 1000, 1200, 1500, and 1800 hours.

speeds characteristic of this episode. Indeed, unusually high simulated nighttime concentrations of tracer pollutant and secondary species are predicted in a vast region the domain. The authors attribute this underestimate of vertical mixing to the absence of consideration for the effects of urban heat islands and mechanical mixing near roadways in the calculation of diffusion parameters. The authors incorporated changes to the model, included in this study, to promote mixing up to the height of the inversion layer during evening hours.

The air quality episode presents several interesting challenges to the modeling community. However, the model is reasonably well behaved in the region were the majority of monitoring stations exists. Furthermore, the overall model response is adequate for the purposes of the current study, i.e. comparison of the Base Case simulation to simulations including chlorine chemistry.

3.2 Sea-salt particles loads

This section provides several characteristics of the sea-salt particle loadings in the South Coast Air Basin of California as predicted by the CIT Airshed Model. In doing so, this section also evaluates the performance of the sea-salt aerosol source functions. Values and plots are presented for a simulation, similar to the Base Case, which now incorporates the complete gas-phase chlorine chemistry mechanism and four of the heterogeneous/multiphase reactions (6 & 9–11). This simulation is denoted as the 'Case Cl Chem' simulation. The extent of chloride depletion with and without the additional chlorine chemistry is also discussed.

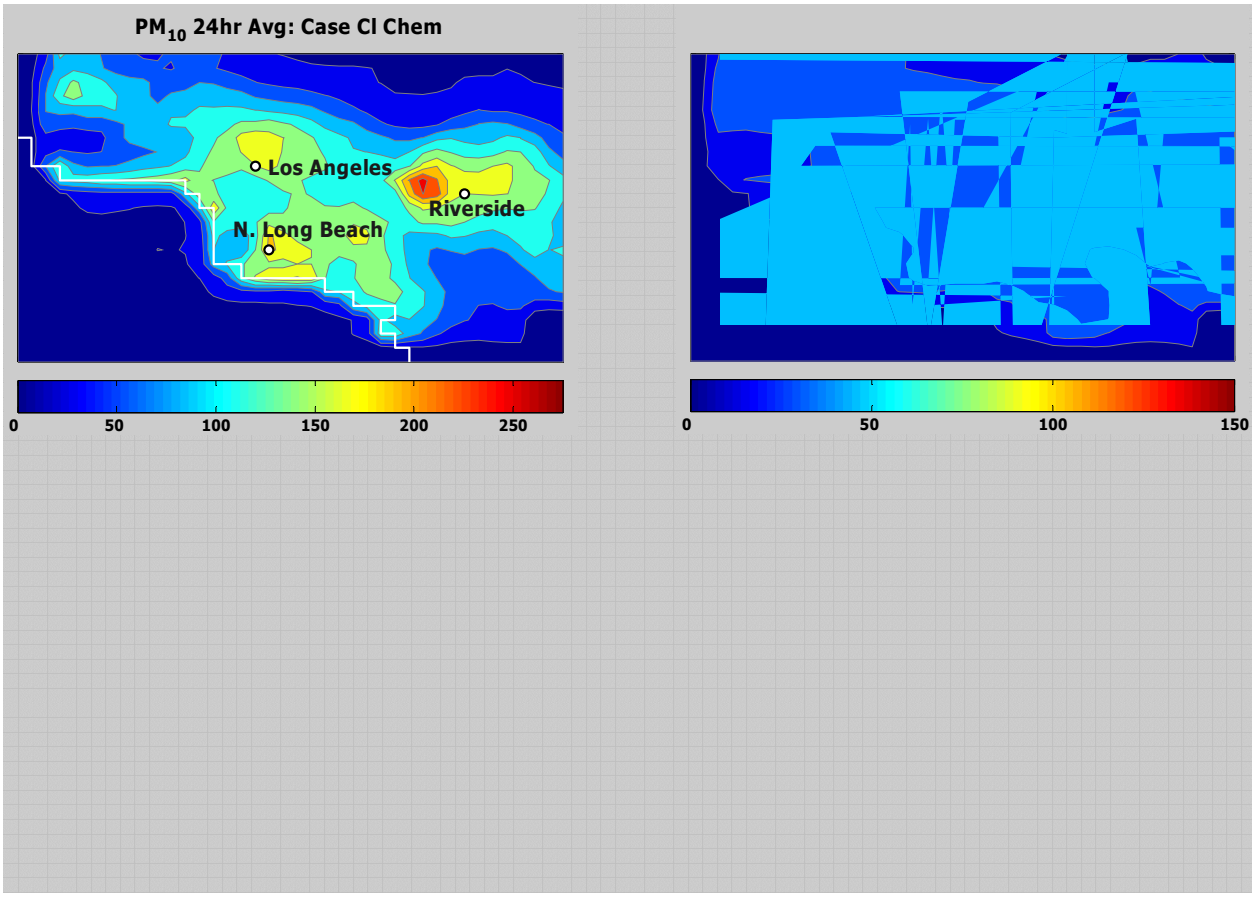

Figure 5: Twenty-four-hour average aerosol concentration contours – 'Case Cl Chem' simulation: September 9, 1993 (all units in $\mu g/m^3$). Shown are model predictions for 24-hour average total PM_{10} concentration, 24-hour average total $PM_{2.5}$ concentration, 24-hour average PM_{10}-chloride concentration, and 24-hour average $PM_{2.5}$-chloride concentration.

Figure 5 shows results for twenty-four hour average PM_{10} and $PM_{2.5}$ total and aerosol chloride mass. Aerosol chloride concentrations are dominated by the surf-zone production of sea-spray; the open-ocean contribution to coastal aerosol concentrations is negligible. Figure 5 also illustrates how higher sea-salt aerosol concentrations are generated in coastal regions that are oriented in line with the general west-to-east wind patterns of the air basin as surf-zone generated aerosol accumulates in these regions.

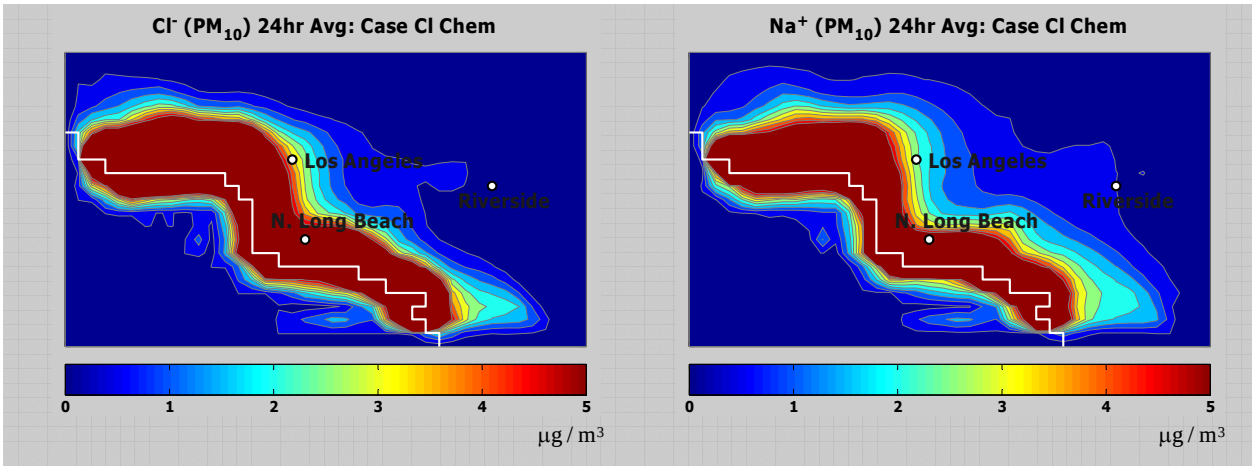

Figure 6: Twenty-four-hour average aerosol concentration contours capped at 5 $\mu g/m^3$ – 'Case Cl Chem' simulation: September 9, 1993 (all units in $\mu g/m^3$). Shown are model predictions for 24-hour average PM_{10}-chloride concentrations capped at 5 $\mu g/m^3$ and 24-hour average $PM_{2.5}$-chloride concentrations capped at 5 $\mu g/m^3$.

In order to demonstrate the reach of sea-salt aerosol inland into the urban airshed, Figure 6 shows 24-hour average PM_{10} sodium and chloride concentration contours capped at 5 $\mu g/m^3$. Although sea-salt aerosol does extend for several tens of kilometers inland, concentrations are quite low. Most of the sea-salt aerosol mass produced in coastal regions is produced as larger particles that settle/deposit fairly quick. Table 4 compares observed versus modeled particulate matter concentration at locations in Long Beach and Claremont, approximately 10 km north and 50 km northeast of the nearest coast. During the observation, total suspended particulate matter (TSP) concentrations were measured instead of actual PM_{10} concentrations. However, due to gravitational settling of very large particles, most of the sodium mass should be within the modeled bins (diameters ≤ 10 µm) at fetches this far from the coast. The results from the comparison suggest that sea-salt particles are modeled well by the CIT Airshed Model and the

newly integrated sea-salt particles source functions. The underestimation of vertical mixing mentioned earlier is a possible explanation of the prediction of sodium concentrations lower than observed values at the Claremont site.

Remote marine boundary layer aerosol populations consist of approximately 100–300 particles, with 5 to 30 particles being directly emitted sea-salt particles [*Seinfeld and Pandis*, 1998 and references therein]. Figure 7 shows a 24-hour-averaged aerosol size distribution approximately 15 km from the coast. The results are consistent with the character of a marine aerosol population influenced by relatively close urban region. The low sea-salt concentrations are indicative of the low wind speeds of the episode. The larger size bins consist mostly of marine-aerosol constituents, non-sea-salt (nss) sulfate, nitrate, organics and unclassified material (e.g., dust). The smaller size bins are dominated by nss-sulfate, organics and unclassified material.

Table 4: Comparison of observed and predicted particulate sodium concentrations (all units in $\mu g/m^3$)

	Long Beach		**Claremont**	
	$PM_{2.5}$-sodium	**TSP-sodium**	**$PM_{2.5}$-sodium**	**TSP-sodium**
Observed	0.50	**3.11**	**0.64**	**1.09**
		PM_{10}-sodium		**PM_{10}-sodium**
Modeled	0.91	2.65	0.28	0.62

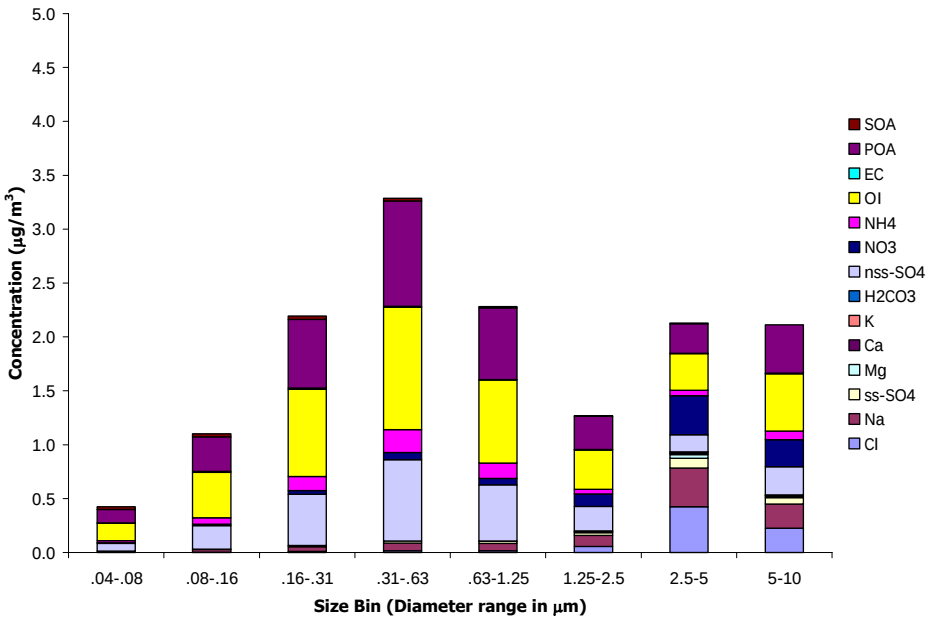

Figure 7: Open-ocean aerosol distribution

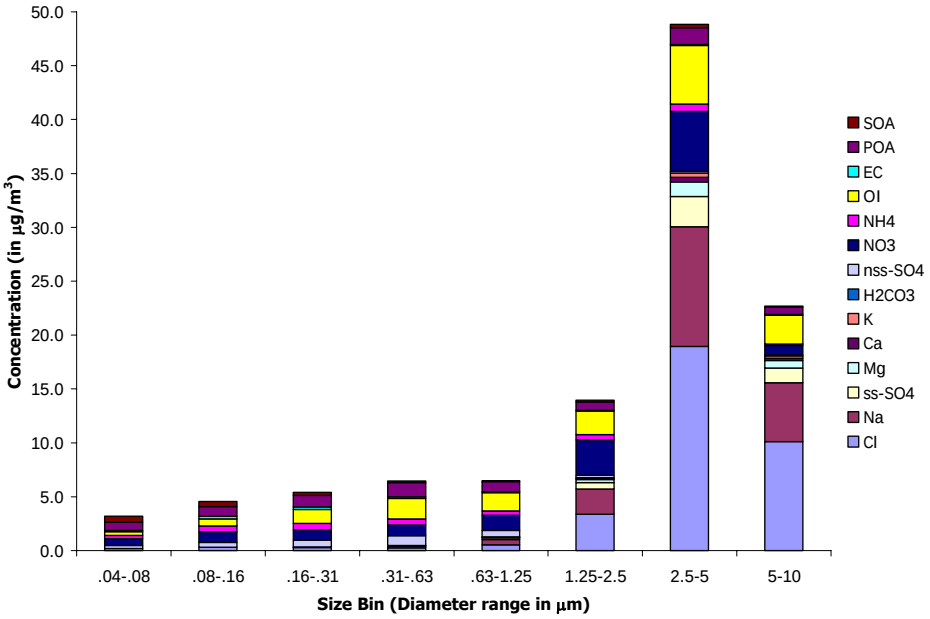

Figure 8: Coastal aerosol distribution

Figure 8 shows a 24-hour-averaged aerosol size distribution in a costal region. Both the urban and marine components of the distribution are increased compared to the more distant oceanic distribution. The concentration of the marine aerosol constituents in the larger bins are greatly enhanced as a result of the surf-zone functions as developed by *De Leeuw et al.* [2000] for conditions off the California coast. Thus, these values are consistent with their observation of enhancement of sea-salt particle concentrations by one to two orders of magnitude over the surf region.

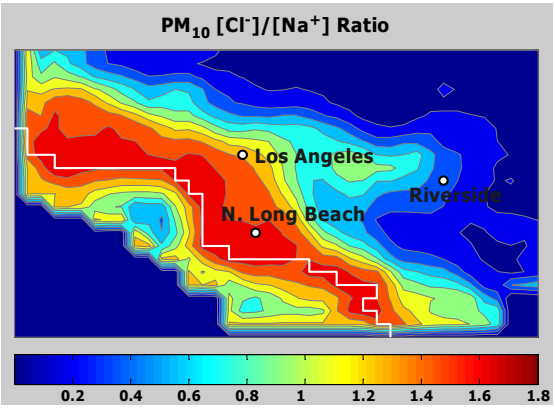

Figure 9: Aerosol PM_{10}-chloride to PM_{10}-sodium ratios. Fresh sea-salt particle ratio ≈ 1.8.

A freshly ejected sea-salt particle is expected to have a mass concentration ratio of chloride to sodium of ~ 1.8. Chloride-to-sodium ratios calculated throughout the basin, shown on Figure 9, illustrate how aerosol particles become depleted in chloride as they travel away from their source. As expected, this chloride depletion is primarily due to acid displacement. As less-volatile stronger acids, such as nitric acid (HNO_3) and sulfuric acid (H_2SO_4), condense onto the aerosol, the lower pH effectively displaces chloride as hydrochloric acid (HCl) gas. In the South Coast Air Basin, displacement occurs primarily by nitric acid. The newly added heterogeneous/multiphase chemical reactions do not significantly affect the rate of acid displacement nor do they enhance aerosol nitrate formation. These results for an episode in early September, 1993, are in qualitative agreement with observations of chloride deficits, attributed to displacement by nitric acid, made for another episode in late September, 1996 [*Gard et al*., 1998; *Hughes et al*., 2000].

3.3 Model results: Cl_2 levels and impact of chlorine chemistry on ozone formation

In the previous section, it was shown that sea-salt aerosol concentrations exhibit generally expected characteristics. The next step in the analysis of the influence of sea-salt aerosol on urban photochemistry is to verify the levels of Cl_2 generated in the model and determine the impact of chlorine chemistry on ozone formation. Figure 10 illustrates that the high levels of molecular chlorine concentrations measured by other investigators in coastal regions cannot be reproduced by the model. The maximum 1-hour average [Cl_2] predicted by the 'Case Cl Chem' simulation is 12 ppt, predicted both in the late evening and at pre-dawn. Whereas *Spicer et al.* [1998] coworkers measured Cl_2 concentrations around 150 ppt in their field campaign, and the mist chamber measurements of *Keene et al.* [1993] suggest Cl_2 concentrations up to 127 ppt, the model predicts concentrations that are an order of magnitude below the observed values. Nonetheless, these values represent an increase by a factor of 30 in the ability to reproduce Cl_2 values when compared to the maximum Cl_2 concentrations predicted by the box model of Spicer and coworkers.

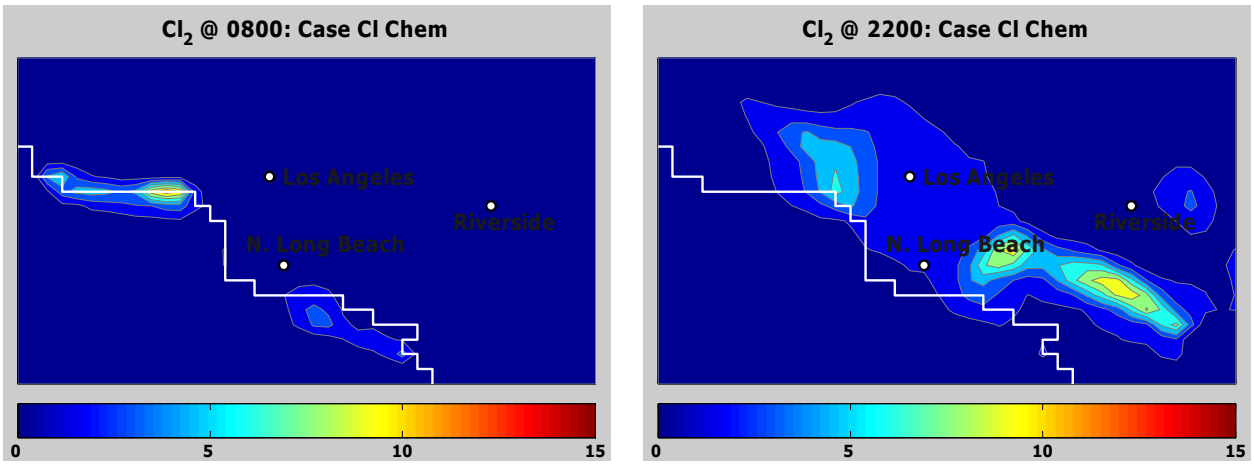

Figure 10: Cl_2 concentration contours for the 'Case Cl-Chem' simulation at 800 and 2200 hours: September 9, 1993 (all units in ppt).

Although the Cl_2 levels are below observed values, an analysis of the influence of the sea-salt derived chlorine chemistry in this simulation on ozone formation dynamics is performed by determining the difference between the concentrations predicted in the 'Case Cl Chem' simulation and the concentrations predicted in the 'Base Case' simulation. Figure 11 exhibits contour plots of this difference throughout the domain at different times on the second day of simulation. These results show that sea-salt chemistry, even when Cl_2 levels are under-predicted, can contribute to ~10 ppb of the ozone concentrations in certain regions. These ozone differences between the simulations are at a maximum in the early hours. Although the influence dissipates in later hours, the fraction of the basin affected by the chlorine chemistry increases due to the influence of various physicochemical processes, with transport being the dominant process. The influence of the chlorine chemistry on the peak grid ozone concentrations and to the peak concentrations at monitoring stations is discussed after presenting the results for three additional modeling scenarios.

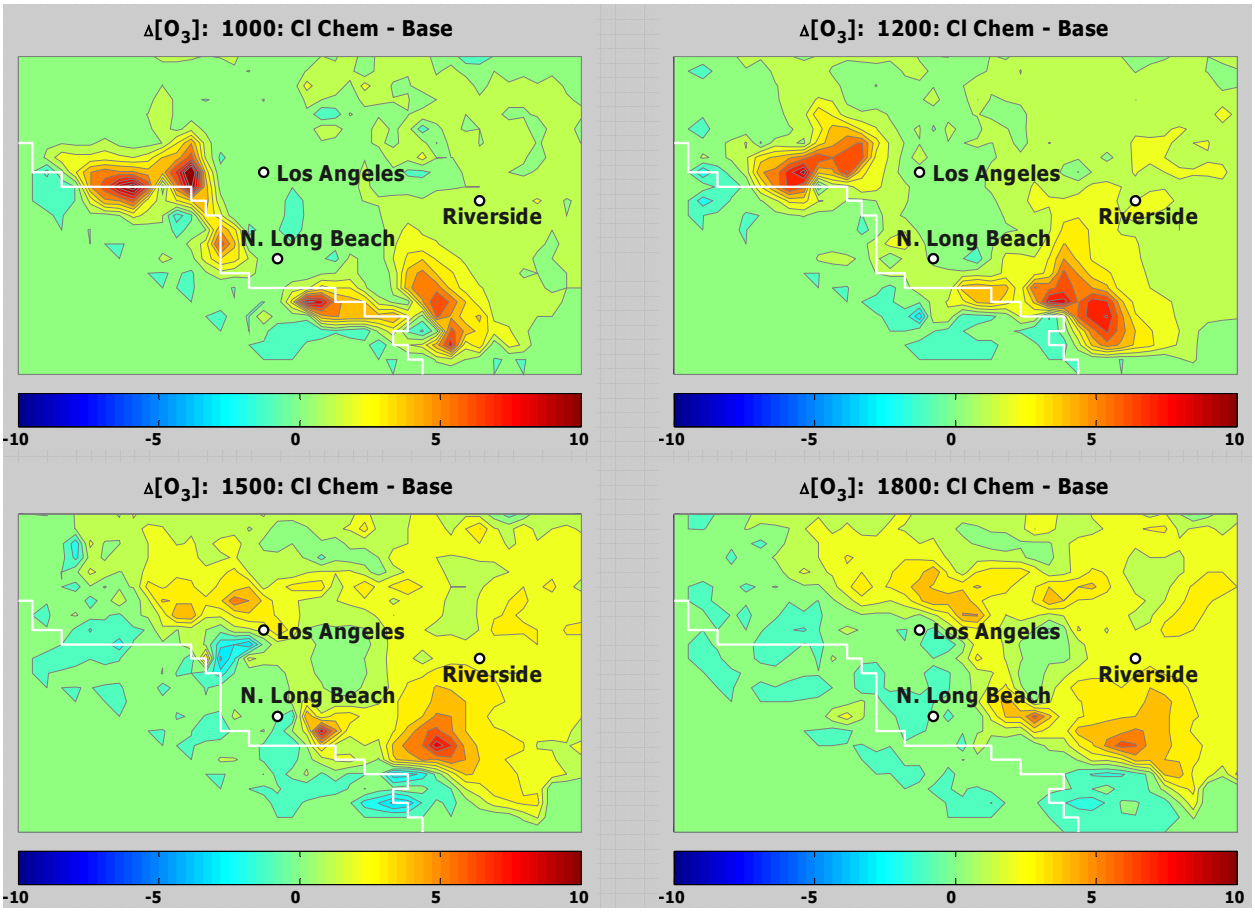

Figure 11: Ozone concentration difference contours: September 9, 1993 (all units in ppb). Shown are diagrams illustrating the value obtained by subtracting ozone concentrations predicted by the 'Case Cl Chem' simulation from ozone concentrations predicted by the 'Base Case' simulation at 1000, 1200, 1500 and 1800 hours.

3.4 Additional Simulations

The results presented for the 'Case Cl Chem' simulation provide a general assessment of the effect of sea-salt derived chlorine chemistry on photochemical smog formation. However, there are still issues that need to be addressed. For instance, molecular chlorine concentrations predicted in the simulation are an order of magnitude lower than expected from values from field measurement data. In addition, these simulations lack the contribution of anthropogenic sources of chlorine. These sources may raise photochemically active chlorine levels not only near the coast but throughout the model domain.

The field measurement and model analysis of *Spicer et al.* [1998] suggested the existence of an unexplained nighttime source of molecular chlorine in coastal regions that allowed for nocturnal accumulation of chlorine up to pre-dawn hours. A reaction of sea-salt particles with the nitrate radical, similar to that of the reaction with the hydroxyl radical, is included in the model (see Reaction 11). The possibility of this reaction occurring as parameterized, or the extent to which it may occur, is uncertain. There is evidence of a similar reaction of the nitrate radical on dilute NaCl solutions and dry NaCl [*Rudich et al.,* 1996*; Seisel et al.,* 1997; *Gershenzon et al.,* 1999] leading to formation of chlorine atoms. The nitrate radical is the principal nighttime oxidant in the atmosphere. Thus, notwithstanding the uncertainties, this modeling scenario, denoted as 'Case Cl Chem & NO_3 Reaction,' provides a sensitivity analysis of the impact of a nighttime mechanism for chlorine build-up.

Figure 12 illustrates that incorporation of this reaction increases the prediction of Cl_2 to values more consistent with the measurements of *Spicer et al.* [1998] and *Keene et al.* [1993]. In a few small areas, the predicted values (~600 ppb) actually exceed by a factor of 4 those measured by the field campaigns, but good agreement is obtained in general. The increase of Cl_2 does not endure past the dawn, when photolysis of both NO_3 and Cl_2 bring the molecular chlorine concentration down to similar levels as the 'Case Cl Chem' simulation as shown in Figure 13. Consequently, the impact of adding the nitrate radical reaction on the sea-salt particles on ozone concentrations is not as marked as the impact witnessed on pre-dawn Cl_2 concentrations. Morning differences between ozone predictions in this scenario versus the 'Base Case' are increased by < 2 ppb in coastal regions when compared to those illustrated on Figure 11 for the 'Case Cl Chem' simulation, with the effect lessening throughout the day. Overall, the same general behavior in ozone formation dynamics is exhibited by the 'Case Cl Chem & NO_3 Reaction' simulation as the 'Case Cl Chem' simulation.

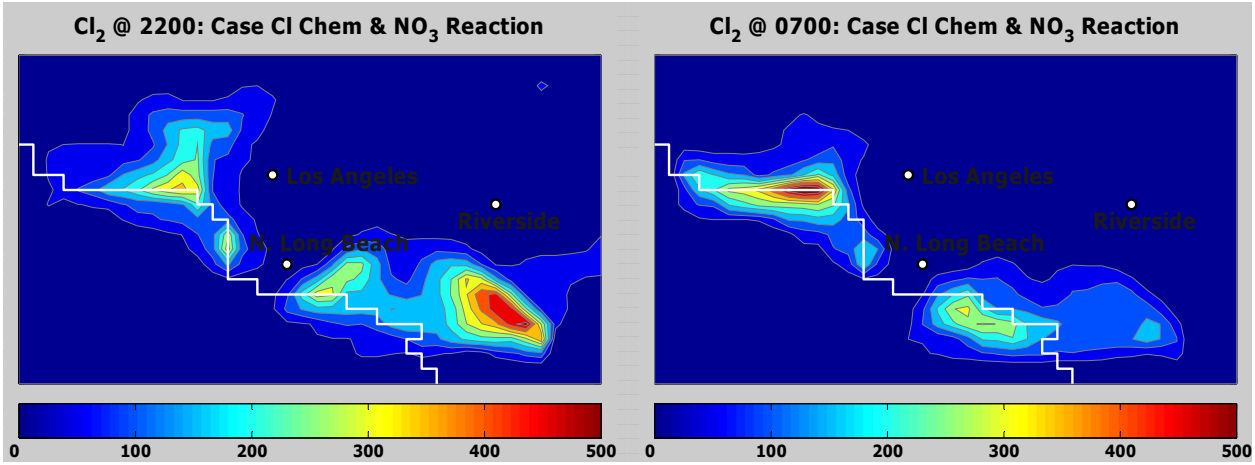

Figure 12: Cl_2 concentration contours for the 'Case Cl-Chem & NO_3 Reaction' simulation at 2200 and 700 hours: September 9, 1993 (all units in ppt).

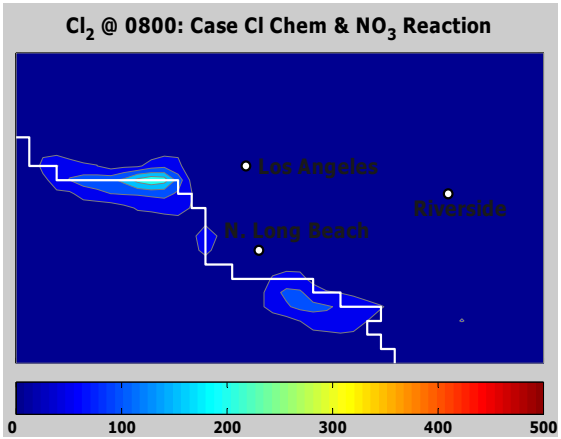

Figure 13: Cl_2 concentration contours for the 'Case Cl-Chem & NO_3 Reaction' simulation at 800 hours: September 9, 1993 (all units in ppt).

The purpose of the current project is to estimate the influence of sea-salt particles on ozone formation in the South Coast Air Basin of California. However, studies in Texas indicate that the contribution of anthropogenic sources of chlorine may also be of concern [*Tanaka et al.,*, 2000]. Potential anthropogenic sources of Cl_2 and HOCl include direct emission from industrial activities, emission from the use of biocides in cooling towers, emission from water and wastewater treatment, and emission from swimming pool treatment. In view of these studies, we have performed additional simulations in order to estimate the impact of an increased burden of reactive chlorine on smog formation in the South Coast Air

Basin of California. Two additional simulations are performed: a simulation prescribing a constant Cl_2 concentration of 150 ppt in all grid cells on all levels, denoted as '$[Cl_2]$ = 150 ppt', and a simulation where the constant Cl_2 concentration is prescribed at an extreme value of 1500 ppt in all levels, designated '$[Cl_2]$ = 1500 ppt'.

Figures 14 – 16 illustrate the effect of both sea-salt aerosol simulations and the two constant-Cl_2 simulations on the concentration of ozone along the "Strip" shown in Figure 2. The "Strip" begins in the Pacific, crosses above the Santa Monica Mountains, passes through central Los Angeles and

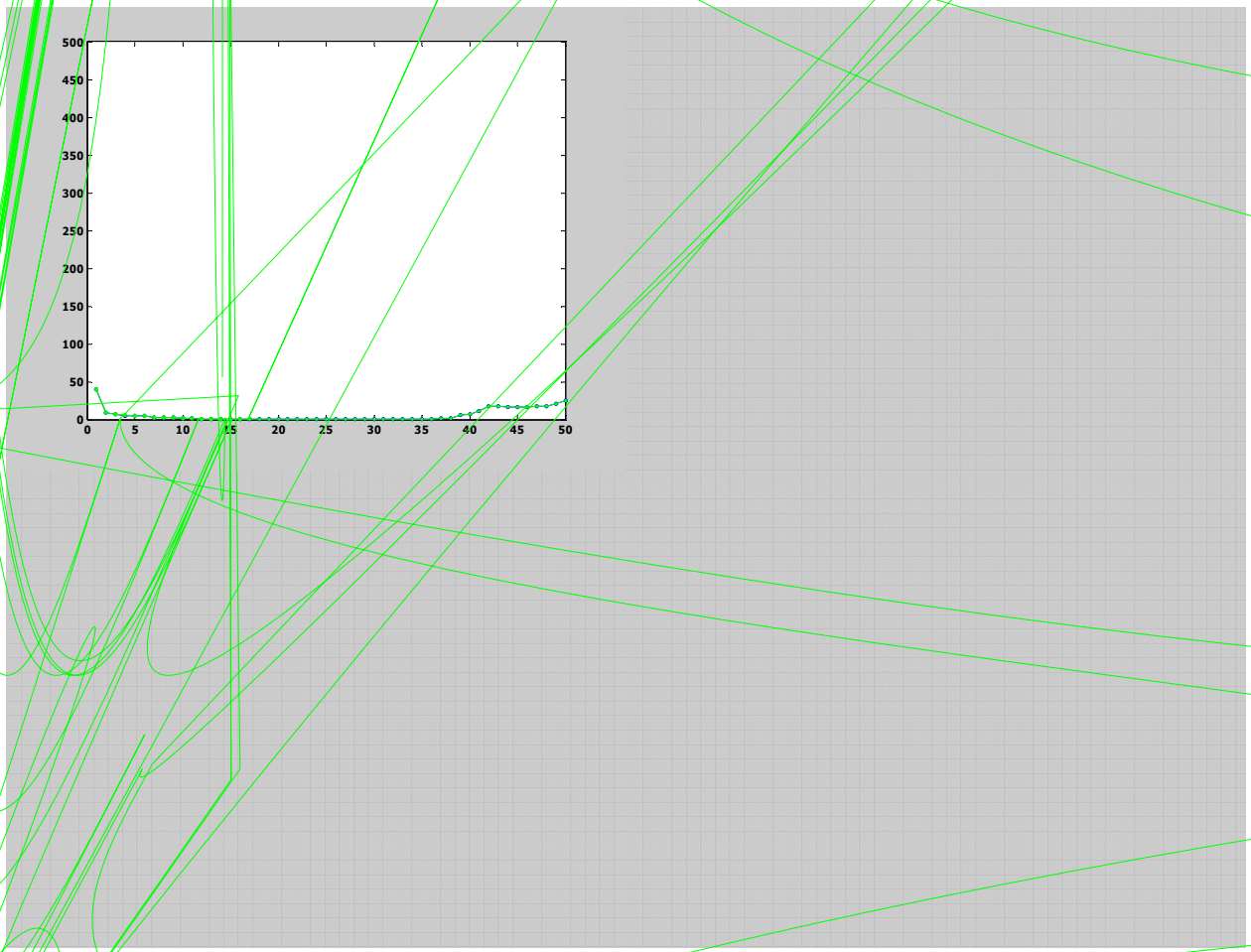

Figure 14: Ozone contour slices for September 8, 1993 at 700, 1000, 1200 and 1500 hours. Illustrated are cross-sections of ozone concentration contours (for each simulation in the study) along a strip of cells shown in Figure 2. The strip of cells begins in the western boundary of the domain in the Pacific Ocean in CIT Cell Number 500 and extends westward above the Santa Monica Mountains, passes through Central Los Angeles, continues towards Riverside and exits through the San Bernardino National Forest.

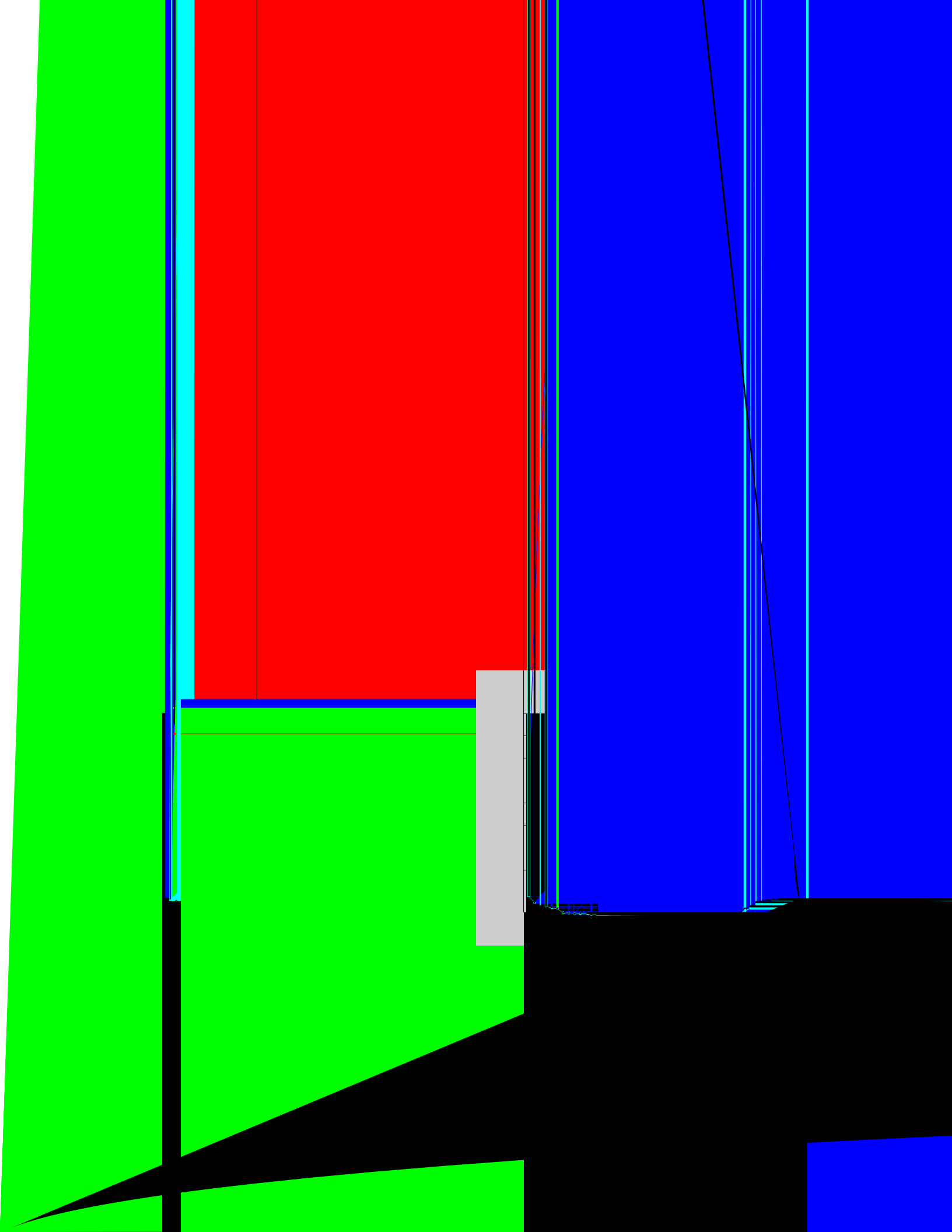

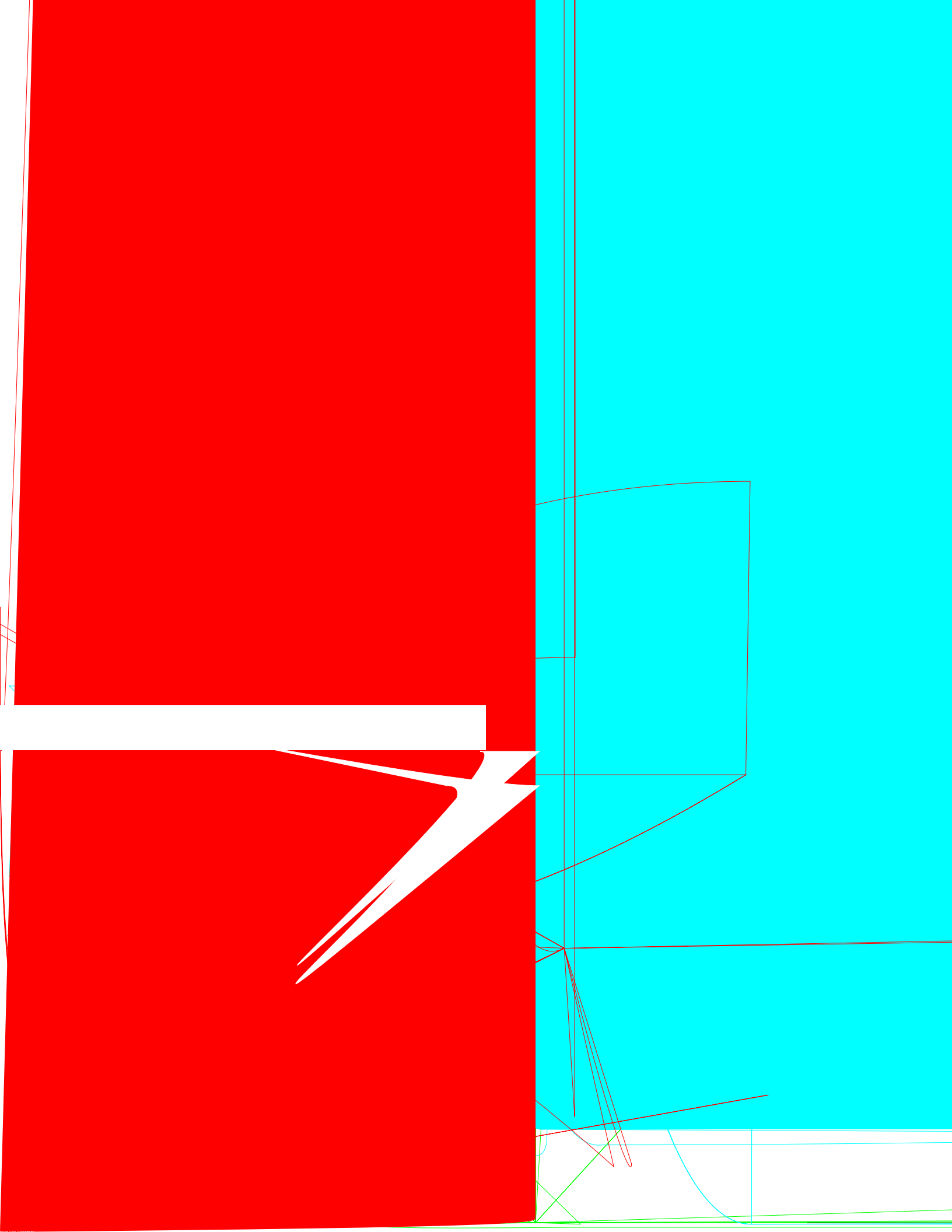

4. Discussion

This section expands on the results presented in the previous section by interpreting the data and discussing its major implications. The ozone contour plots in the previous section provide a broad impression of the general effects of chlorine chemistry. In brief, ozone concentrations are increased near the coast shortly after sunrise. The effect dissipates as the day continues but the physicochemical processes simulated in the model, primarily transport, convey its influence throughout the region. In order to grasp the effect on specific locations of the South Coast Air Basin, Table 5 provides different parameters that evaluate the impact of chlorine chemistry on ozone as exhibited in all scenarios.

Table 5 lists 36 monitoring stations in the South Coast Air Basin of California. Some of the stations (e.g., Banning, Hemet, Hesperia, Perris, Redlands, and San Bernardino) are contained in the northeastern area of the domain where model limitations, caused by the meteorological conditions of the chosen episode, resulted in overly high ozone concentrations as discussed in Section 3.1. However, the overall model response is adequate for the purposes of this study. The table is generated by analyzing 1-hour average concentrations, in units of ppb, as predicted by the model.

The first column entry in the Table, after the station names, provides the peak ozone concentration at every station calculated by the 'Base Case' simulation. The following four columns list the 'Δ Peak 1-hr $[O_3]$' – deviations from the peak 'Base Case' $[O_3]$ when compared to the peak $[O_3]$ predicted by each of the other modeling scenarios, respectively, at that location. The final four columns provide the 'Max 1-hr Δ $[O_3]$' – the maximum difference *at any hour* when comparing ozone predictions of the 'Base Case' to each of the other scenarios, respectively, at that location. Calculations of these parameters are also provided for the entire domain and for a station-wide summary. In addition, the 'Max 1-hr Δ $[O_3]$' parameter is also given for grid-cells having ozone concentrations over 80 and 90 ppb.

For the 'Case Cl Chem' simulation, the peak ozone concentration at all stations increases by an average of 2.3 ppb, with stations in Glendora and El Toro elevating their $[O_3]$ by ~ 4 ppb. The station predicting the highest ozone peak for this simulation, as well as for the 'Base Case,' is located at Hemet.

Table 5: Summary of ozone metrics at 36 stations of the South Coast Air Basin of California (all values in units of ppb)

Monitoring Stations		Peak [O_3]	Δ Peak 1-hr [O_3]				Max Δ 1-hr [O_3]			
		Base Case	Case 1	Case 2	Case 3	Case 4	Case 1	Case 2	Case 3	Case 4
ANAH	Anaheim	65.9	2.6	3.6	87.2	253.8	3.6	4.2	87.2	270.0
AZUS	Azusa	93.6	2.2	3.0	96.3	498.0	2.7	3.5	117.4	532.1
BANN	Banning	352.0	2.1	2.2	52.7	-71.8	3.5	3.1	60.2	111.1
BURK	Burbank	127.0	3.8	3.5	83.0	267.7	4.7	4.4	85.5	302.2
CELA	Central LA	102.5	3.0	4.5	70.6	323.8	3.6	4.5	74.8	369.9
CLAR	Claremont	151.3	2.7	3.1	119.7	232.9	3.2	4.0	127.2	271.1
COST	Costa Mesa	116.3	3.5	2.1	10.4	39.0	4.5	5.3	21.4	103.3
CRES	Crestline	242.7	2.1	2.7	70.6	-1.7	2.7	3.0	70.6	99.3
ELRO	El Rio	40.0	0.0	0.0	0.0	0.0	0.3	0.1	1.2	0.0
FONT	Fontana	181.0	1.6	2.2	102.5	224.1	2.8	3.3	107.8	251.3
GLEN	Glendora	126.4	4.1	3.2	132.8	440.3	4.2	4.2	136.3	478.4
HAWT	Hawthorne	82.0	0.7	0.0	8.9	33.2	1.4	1.4	16.0	85.5
HEME	Hemet	353.3	2.2	2.3	40.6	-112.0	2.2	2.3	40.6	58.7
HESP	Hesperia	336.6	-0.5	0.9	3.5	-126.7	2.2	1.9	50.4	42.0
LAHB	La Habra	50.1	2.4	2.4	87.6	327.1	2.4	2.4	90.9	343.5
LGBH	North Long Beach	50.7	1.3	1.7	26.4	163.7	1.3	1.7	28.9	190.6
LSAL	Los Alamitos	82.5	2.2	3.5	58.1	230.4	2.7	4.4	58.1	268.6
LYNN	Lynwood	67.5	0.7	-1.2	23.5	181.3	0.8	1.2	35.5	207.9
NEWL	Newhall	134.8	1.5	1.7	102.3	113.7	1.6	1.7	102.3	158.0
NORC	Norco	195.7	2.8	2.9	64.8	99.3	3.4	3.5	107.7	161.5
PASA	Pasadena	55.0	2.1	2.9	105.1	484.4	4.9	5.2	113.8	484.7
PERI	Perris	307.1	3.0	2.9	65.1	-70.7	3.5	3.5	68.5	52.1
PICO	Pico Rivera	84.6	2.5	2.2	64.6	309.4	2.6	2.6	76.0	355.8
PIRU	Piru	95.1	1.1	1.3	69.8	87.4	2.1	2.4	72.6	99.9
PLSP	Palm Springs	205.7	3.3	3.1	85.0	48.2	3.3	3.1	85.0	140.9
POMA	Pomona	129.4	2.9	3.1	98.3	306.3	2.9	3.6	114.6	347.9
RDLD	Redlands	326.5	2.9	3.1	80.1	98.6	3.4	4.9	80.1	104.3
RESE	Reseda	118.8	3.3	3.1	89.2	159.5	3.3	3.2	92.4	203.0
RIVR	Riverside	285.9	2.5	2.3	74.8	38.3	2.6	2.6	97.6	115.6
SIMI	Simi Valley	82.2	2.0	2.1	76.6	165.5	2.8	2.5	88.7	181.2
SNBO	San Bernardino	313.7	3.4	3.3	88.9	86.9	3.4	3.3	90.1	136.0
THSO	Thousand Oaks	38.2	1.6	1.3	47.5	163.0	1.6	1.3	47.5	181.1
TORO	El Toro	166.3	4.0	3.1	46.1	166.9	7.7	7.4	57.1	232.9
UPLA	Upland	162.6	2.6	2.7	108.8	186.0	2.9	3.6	117.8	228.1
WHIT	Whittier	68.7	1.9	2.4	77.0	327.6	1.9	2.4	83.3	365.9
WSLA	West LA	81.1	3.2	3.2	23.1	85.3	3.2	3.6	23.1	127.8
	Station-wide*		2.2	2.3	53.3	238.3	7.7	7.4	136.3	532.1
	Domain		3.9	3.8	62.7	195.1	12.7	13.7	139.2	538.1
	Domain over 80 ppb						12.5	11.5	139.2	538.1
	Domain over 90 ppb						11.7	9.6	139.2	538.1
	Station-wide peak (location)	353.3 HEME	355.5 HEME	355.6 HEME	406.6 RDLD	591.6 AZUS				
	Domain peak	406.2	410.1	410.0	468.9	601.3				

1: Case Cl Chem; 2: Case Cl Chem & NO_3 Reaction; 3: Case [Cl_2] =150 ppt; 4: Case [Cl_2] =1500 ppt

* Δ 1-hr peak station-wide [O_3] (not necessarily same location) and maximum of 1-hr Δ [O_3] at any station at any time

The station-wide peak ozone increases by 2.2 ppb and the domain peak [O_3] increases by 3.9 ppb. The 'Max 1-hr Δ [O_3]' demonstrates that ozone concentrations may increase by greater amounts at times that do not coincide with the peak ozone concentrations, with this value averaging 2.9 ppb over all stations. The highest 1-hr increase is predicted in El Toro at 7.7 ppb. The highest increase in ozone in the domain at any grid cell at any hour is predicted to reach 12.7 ppb. If the analysis is limited only to cells exceeding the state 1-hr [O_3] standard of 90 ppb, then the highest 1-hr ozone increase is calculated at 11.7 ppb.

The 'Case Cl Chem & NO_3 Reaction' predicts much higher pre-dawn Cl_2 concentrations than the 'Case Cl Chem simulation,' with concentrations exceeding 600 ppt in a small region as shown previously in Figure 12. However, the effect on O_3 concentrations predicted by the model is not as sizeable as may be expected. Peak ozone concentration at all stations increase by an average of 2.4 ppb compared to the 'Base Case', with the station in Central LA increasing its [O_3] by ~4.5 ppb. Twenty-five stations increase their ozone concentration by an average of ½ ppb compared to the 'Case Cl Chem.' Eleven stations exhibit a slight decrease averaging 0.2 ppb. The station-wide peak ozone, again located in Hemet, and the domain peak ozone remain within 0.1 ppb of the values predicted by the 'Case Cl Chem' simulation. The average 'Max 1-hr Δ [O_3]' predicted by the 'Case Cl Chem & NO_3 Reaction' scenario is 3.2 ppb, with the highest single-hour increase in ozone again predicted in El Toro at 7.4 ppb. The highest increase in ozone in the domain at any grid cell at any hour is predicted to reach 13.7 ppb. Upon limiting the analysis to cells exceeding an ozone concentration of 90 ppb, the highest one-hour increase in [O_3] is 9.7 ppb.

The ozone parameters defined above are also given in Table 5 for the simulations prescribing a constant chlorine concentration throughout the domain. These simulations, although not representative of the real troposphere, provide insight on the nature of chlorine chemistry and suggest on the effect of additional basin-wide sources of chlorine. In brief, for the 'Case [Cl_2]=150 ppt' simulation, ozone concentrations are increased significantly throughout the domain, with almost all stations reporting peak ozone increases above 50 ppb and a few above 100 ppb. For the 'Case [Cl_2] =1500 ppt' scenario, ozone concentrations are increased throughout a large portion of the domain during the entire day. New ozone

peaks develop and temporal and spatial dynamics are affected altogether. Overall, ozone levels are unrealistically high in this simulation that can only represent a modeling exercise.

The results presented in the previous and present section generates an interesting query: Why do ozone concentrations remain fairly unaffected in the 'Case Cl Chem & NO_3 Reaction' simulation when compared to the 'Case Cl Chem' simulation? A rigorous answer to this question can only be obtained through sensitivity analysis of the chemical mechanism with respect to the modeling episode in question. However, an analysis of the relative concentration of OH and Cl radicals in each simulation yields some interesting results.

Table 6: Comparison of several [OH], [Cl_2], and [Cl] metrics as predicted by the simulations

Maximum individual-cell 1-hr average concentrations*

Species		Base	Case 1	Case 2	Case 3	Case 4
[OH]	molecule cm^{-3}	1.70×10^7	1.70×10^7	1.70×10^7	1.78×10^7	2.91×10^7
[Cl_2]	Ppt		11.99	637.10	150.00	1500.00
[Cl]	molecule cm^{-3}		3.44×10^4	3.13×10^4	4.56×10^5	1.65×10^7

Maximum domain-averaged 1-hr average concentrations**

Species		Base	Case 1	Case 2	Case 3	Case 4
[OH]	molecule cm^{-3}	5.58×10^6	5.62×10^6	5.63×10^6	7.25×10^6	1.02×10^7
[Cl_2]	ppt		1.45	74.74	150.00	1500.00
[Cl]	molecule cm^{-3}		1.94×10^3	1.79×10^3	6.74×10^4	1.75×10^6

Maximum individual-cell 24-hr average concentrations***

Species		Base	Case 1	Case 2	Case 3	Case 4
[OH]	molecule cm^{-3}	3.97×10^6	3.98×10^6	3.98×10^6	4.18×10^6	6.41×10^6
[Cl_2]	ppt		4.35	238.00	150.00	1500.00
[Cl]	molecule cm^{-3}		5.46×10^3	6.70×10^3	6.29×10^4	2.06×10^6

Domain-averaged 24-hr average concentrations

Species		Base	Case 1	Case 2	Case 3	Case 4
[OH]	molecule cm^{-3}	1.51×10^6	1.53×10^6	1.53×10^6	1.95×10^6	3.01×10^6
[Cl_2]	ppt		0.68	27.35	150.00	1500.00
[Cl]	molecule cm^{-3}		3.82×10^2	4.25×10^2	1.82×10^4	4.23×10^5

1: Case Cl Chem; 2: Case Cl Chem & NO_3 Reaction; 3: Case [Cl_2] =150 ppt; 4: Case [Cl_2] =1500 ppt

* Values do not necessarily correspond to the same cell for this parameter or the same hour.

** Values do not necessarily correspond to the same hour.

*** Values do not necessarily correspond to the same cell.

Table 6 provides several metrics of the concentrations of Cl_2, OH and Cl encountered in the model. Included (in top to bottom order) is the maximum 1-hour average concentrations predicted at

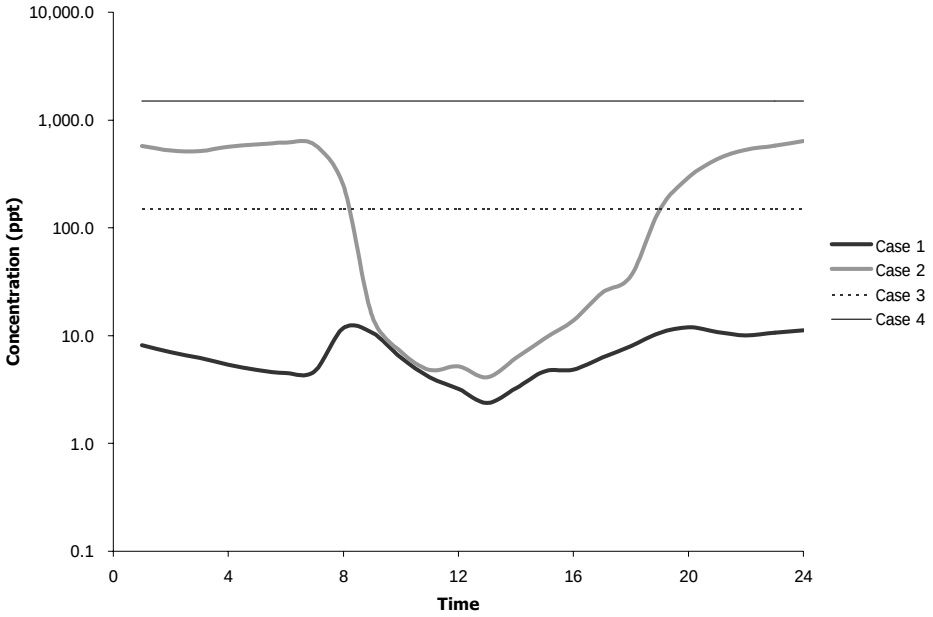

Figure 17: Time series: Maximum individual-cell 1-hr average Cl_2 concentrations

1: Case Cl Chem; 2: Case Cl Chem & NO_3 Reaction; 3: Case $[Cl_2]$ =150 ppt; 4: Case $[Cl_2]$ =1500 ppt
** Values do not necessarily correspond to the same cell

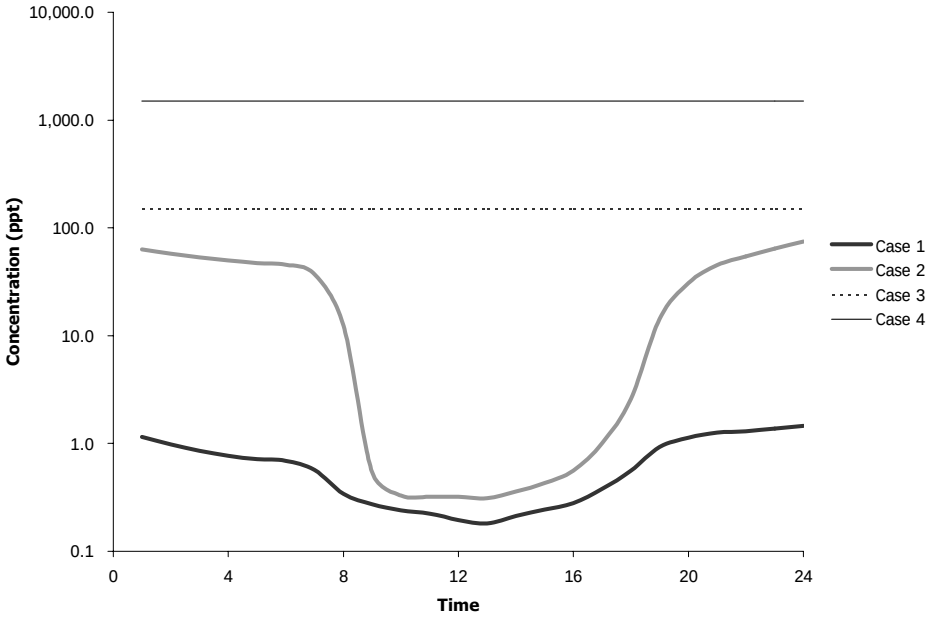

Figure 18: Time series: Domain-averaged 1-hr average Cl_2 concentrations

1: Case Cl Chem; 2: Case Cl Chem & NO_3 Reaction; 3: Case $[Cl_2]$ =150 ppt; 4: Case $[Cl_2]$ =1500 ppt

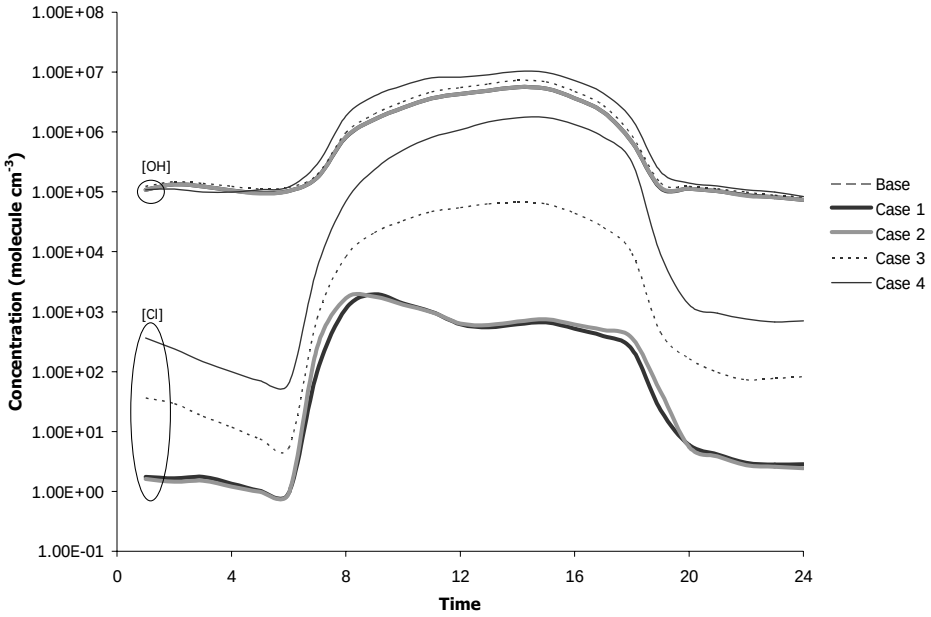

Figure 19: Time series: Domain-averaged 1-hr average OH and Cl concentrations

1: Case Cl Chem; 2: Case Cl Chem & NO_3 Reaction; 3: Case $[Cl_2]$ =150 ppt; 4: Case $[Cl_2]$ =1500 ppt

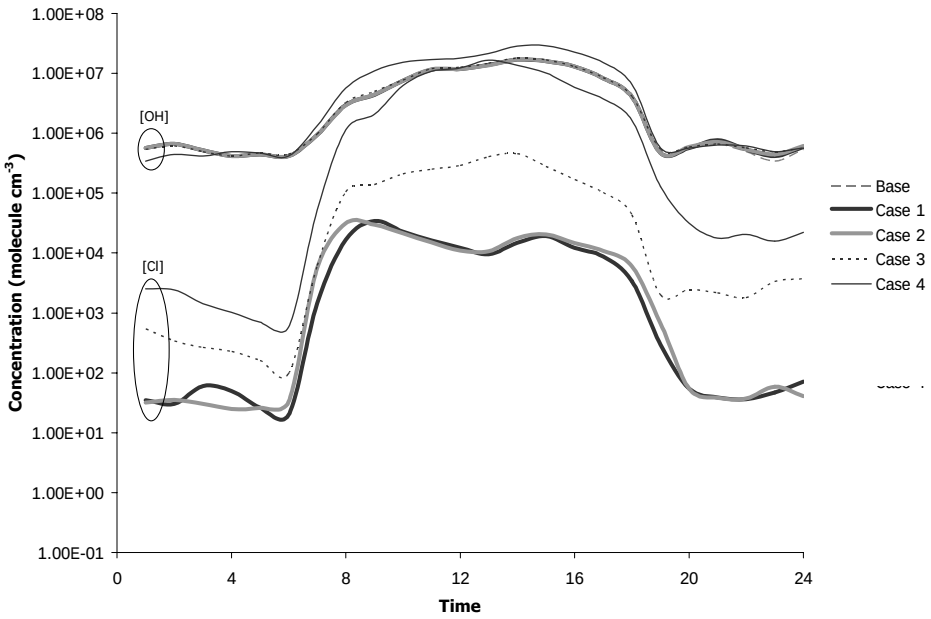

Figure 20: Time series: Maximum individual-cell 1-hr average OH and Cl concentrations

1: Case Cl Chem; 2: Case Cl Chem & NO_3 Reaction; 3: Case $[Cl_2]$ =150 ppt; 4: Case $[Cl_2]$ =1500 ppt
** Values do not necessarily correspond to the same cell

any location at any hour, the maximum *domain-averaged* 1-hour average concentration value predicted at any hour, the maximum 24-hour average concentration predicted at any location, and the domain-averaged 24-hour average concentration. Figures 17–20 illustrate the temporal variation of the maximum individual-cell concentrations and domain-averaged 1-hr concentrations.

Peak and 24-hour average hydroxyl concentrations are in good agreement with literature values [*Seinfeld and Pandis,* 1998; *Finlayson-Pitts and Pitts,* 2000]. Maximum individual-cell hydroxyl concentrations reach 1.70×10^7 molecule cm^{-3} and the domain-averaged OH concentration peaks at 5.6×10^6 molecule cm^{-3} during the early afternoon. Maximum individual cell 24-hour average hydroxyl radical concentrations are predicted at 4.0×10^6 molecule cm^{-3} and at 1.5×10^6 molecule cm^{-3} for the domain-average.

Domain-averaged nighttime OH radical concentrations are predicted at $\sim 1 \times 10^5$ molecule cm^{-3}. Maximum individual cell nighttime hydroxyl concentrations are predicted at $\sim 5 \times 10^5$ molecule cm^{-3}. Anomalously high nighttime levels of OH concentrations have been measure over forest regions up to concentrations of $\sim 1 \times 10^6$ molecule cm^{-3} [*Faloona et al.*, 2001]. However, the nighttime OH predictions by the CIT Airshed model are in excellent agreement with other modeling studies aimed at investigating nighttime production of OH radicals [*Bey et al.,* 1997, 2001a, 2001b]. Bey *et al.* [1997, 2001a] predicted nighttime lows for OH concentrations of $\sim 10^5$ molecule cm^{-3} in urban regions, in direct agreement with the domain-averaged value predicted by the CIT Airshed model.

The nighttime mechanism for OH radical production [*Bey et al.*, 1997, 2001b] in urban regions is initiated by the oxidation of volatile organic compounds, mainly alkenes, by ozone and the nitrate radical to form an organic peroxy radical (RO_2) pool. Hydroperoxy radicals (HO_2) are generated from the subsequent reaction of RO_2 with nitric oxide (NO) and from the direct reaction of alkenes with ozone. Hydroxyl radicals are produced primarily from the reaction of HO_2 with NO, with a lesser contribution from the alkene-ozone reactions and a minor contribution from the reaction of HO_2 with ozone. Once formed, hydroxyl radicals can propagate their own formation through oxidation of VOCs to form RO_2

radicals and through reaction with CO to form HO_2 radicals. Given the presence of high residual ozone concentrations of the mechanism and the highly polluted nature of the South Coast Air Basin of California, maximum individual-cell nighttime lows near ~ 5×10^5 are consistent with the analysis of Bey and coworkers.

The principal mechanism leading to ozone formation is well-recognized [*Finlayson-Pitts and Pitts*, 1997, 2000; *Seinfeld and Pandis*, 1998]. Briefly, OH radicals initiate the oxidation of organic compounds leading to formation of organic peroxy (RO_2) and hydroperoxy (HO_2) radicals. These RO_2 and HO_2 radicals oxidize nitric oxide (NO) to nitrogen dioxide (NO_2). Nitrogen dioxide then photolyzes to form ground-state oxygen atom, $O^3(P)$, which undergoes an association reaction with oxygen to form ozone. The chlorine-atom initiated oxidation of organics needs to occur at rates similar to the OH initiated oxidation to influence this mechanism. The rate constants for the reactions of Cl radicals with most organics compounds is 1–2 orders of magnitude faster than the corresponding rate constants for reactions with OH, with many reactions occurring at the collision-controlled rate. Thus, Cl atom concentrations need to be present within ~ 2 orders of magnitude of OH concentrations to play a role in ozone chemistry.

Table 7: Comparison of additional [OH], [Cl_2], and [Cl] metrics as predicted by the simulations

Maximum individual cell 3-hr (6:00 AM – 9:00 AM) average concentrations*						
Species		**Base**	**Case 1**	**Case 2**	**Case 3**	**Case 4**
[OH]	molecule cm^{-3}	4.41×10^6	4.38×10^6	4.41×10^6	5.00×10^6	1.09×10^7
[Cl_2]	ppt		11.75	592.30	150.00	1500.00
[Cl]	molecule cm^{-3}		3.44×10^4	3.13×10^4	4.97×10^4	1.19×10^6
Domain-averaged 3-hr (6:00 AM – 9:00 AM) average concentrations						
Species		**Base**	**Case 1**	**Case 2**	**Case 3**	**Case 4**
[OH]	molecule cm^{-3}	8.45×10^5	8.68×10^5	8.70×10^5	1.05×10^6	2.05×10^6
[Cl_2]	ppt		0.39	16.68	150.00	1500.00
[Cl]	molecule cm^{-3}		1.05×10^3	1.24×10^3	9.87×10^3	1.03×10^5
Maximum individual-cell 8-hr (9:00 AM – 5:00 PM) average concentrations*						
Species		**Base**	**Case 1**	**Case 2**	**Case 3**	**Case 4**
[OH]	molecule cm^{-3}	1.70×10^7	1.70×10^7	1.70×10^7	1.78×10^7	2.91×10^7
[Cl_2]	ppt		6.28	25.10	150.00	1500.00
[Cl]	molecule cm^{-3}		2.27×10^4	2.13×10^4	4.65×10^5	1.65×10^7
Domain-averaged 8-hr (9:00 AM – 5:00 PM) average concentrations						
Species		**Base**	**Case 1**	**Case 2**	**Case 3**	**Case 4**
[OH]	molecule cm^{-3}	3.98×10^6	4.02×10^6	4.02×10^6	5.18×10^6	7.89×10^6
[Cl_2]	ppt		0.24	0.46	150.00	1500.00
[Cl]	molecule cm^{-3}		7.16×10^2	7.55×10^2	4.97×10^4	1.19×10^6

1: Case Cl Chem; 2: Case Cl Chem & NO_3 Reaction; 3: Case [Cl_2]=150 ppt; 4: Case [Cl_2]=1500 ppt
* Values do not necessarily correspond to the same cell.

Figures 19–20 show that peak OH levels are predicted around 2:00 pm for all simulations, whereas peak Cl concentrations are predicted at 8:00 am and 9:00 am for the 'Case Cl Chem & NO_3 Reaction' and the 'Case Cl Chem' scenarios respectively. It is only during morning hours that Cl atoms compete favorably with the OH radical, when coastal concentrations are within a factor of ~130–140 of maximum OH concentrations and a factor of ~25–30 of the domain-averaged [OH]. Chlorine atoms may dominate the oxidation of some organic compounds in this region. However, this predominance is limited to the coast since domain-averaged [Cl] is ~700–800 times lower than domain-averaged [OH]. Table 7 presents domain-averaged and the maximum single-cell concentrations for OH, Cl_2 and Cl averaged from 6:00 am to 9:00 am.

Chlorine radical initiated oxidation of organics cannot compete as favorably with OH initiated oxidation during the remainder of the morning and throughout the afternoon. Coastal Cl concentrations during this period are typically 750–800 times below maximum OH concentrations and 180–190 times below the domain average [OH]. Furthermore, domain-averaged [Cl] is over 5000 times less than domain-averaged [OH]. Table 7 presents domain-averaged and the maximum single-cell concentrations for OH, Cl_2 and Cl averaged from 9:00 am to 5:00 pm.

Figures 19–20 and Table 7 presented in this section show that there is little difference in the evolution of chlorine atom concentration between the 'Case Cl Chem' and the 'Case Cl Chem & NO_3 Reaction' simulations, except for a shift in the timing of the peak concentration. The specific reason for the lack of a more pronounced variation in the predictions eludes simple explanation. Only by thorough testing of the chemical mechanism and sensitivity studies, both beyond the scope of this study, can a precise answer be found.

The results of these simulations suggest that inclusion of sea-salt derived chlorine chemistry in photochemical models may increase morning ozone predictions by as much as ~12 ppb in coastal regions and by ~ 4 ppb to the peak domain ozone in the afternoon. The peak ozone concentrations at most

monitoring sites increases by 2 – 4 ppb and even higher ozone increases, up to 7 ppb, are predicted at other times not coinciding with the peak. Overall, ozone exposure is increased throughout the domain.

These results are more remarkable when compared to the results studies performed for the Texas Natural Resource Conservation Commission (TNRCC) by researchers at the University of Texas, Austin (UT Austin) [*Tanaka and Allen*, 2001; *Chang et al*., 2001, 2002]. Researchers at UT Austin have collected or estimated emissions data from various anthropogenic and natural sources in the Houston Metropolitan Area. The authors estimate that the principal emissions of chlorine in the region emanated from cooling towers (47%), swimming pools (39%) and industrial sources (11%). The authors estimate that emissions from sea-salt particles contribute to only three percent of chlorine emissions. Although the authors recognize that their estimate of sea-salt derived emissions is highly uncertain, their studies indicate that anthropogenic sources are indeed the prevalent source of chlorine in their domain (up to 97%).

The estimates by UT Austin of the contribution of chlorine chemistry to ozone concentrations yield results strikingly similar to the current studies that do not include anthropogenic sources of chlorine [*Chang et al*., 2002]. For various simulation scenarios in late summer, morning ozone predictions are increased by 11–16 ppb. Afternoon maximum ozone differences are in the range of 5–7 ppb and the peak domain ozone increases by 1–3 ppb.

Anthropogenic sources in the South Coast Air Basin of California may contribute significantly to chlorine loads in the atmosphere. Depending on their spatial distribution, these sources may have a greater opportunity to enhance ozone formation by emitting chlorine gases directly into regions rich in hydrocarbons and oxides of nitrogen.

5. Summary and Conclusions

In order to determine the influence of chlorine chemistry on an urban airshed, we present here the first systematic modeling study that addresses two important issues: First, can urban photochemical models that simulate sea-salt particle formation make first-order estimates of observed chlorine levels? Second, how do such chlorine levels affect the formation of ozone in an urban coastal airshed?

The role of the chlorine atom as a potential oxidant of organic compounds in urban coastal areas has received much attention in recent years [*Keene et al.,* 1990; *Finlayson-Pitts,* 1993; *Pszenny et al*., 1993; *Keene et al.,* 1998]. However, urban photochemical models have not included reactions of chlorine chemistry because significant chlorine atom concentrations have not been expected in these regions, thus making its effect on ozone formation minimal [*Jacob,* 2000]. Indeed, the reaction of hydrochloric acid, HCl, with the hydroxyl radical (OH) to form chlorine atoms (Cl) is slow, and most of the chlorine present in fresh sea-salt particles, the principal atmospheric chlorine reservoir, is released to the gas-phase as hydrochloric acid due to displacement by less-volatile stronger acids [*Gard et al.,* 1998; *Hughes et al.,* 2000].

Nonetheless, laboratory studies have shown that sea-salt particles may undergo chemical reactions that lead to the release of photochemical chlorine-atom precursors [*Finlayson-Pitts and Hemminger,* 2000]. Field studies have provided evidence supporting the presence of these photo-labile chlorine species in coastal regions. In particular, molecular chlorine (Cl_2) concentrations up to 150 ppt have been observed [*Keene et al.,* 1993; *Spicer et al.,* 1998]. Heterogeneous/ multiphase chemical reactions on sea-salt particles may enhance daytime chlorine-atom levels beyond that predicted solely due to the gas-phase reaction of hydroxyl radical with hydrochloric acid.

The California Air Resources Board has expressed interest in determining the influence that sea-salt particles have on air quality. Preliminary simulations performed by the ARB suggested that the chlorine radical could significantly impact predicted ozone concentrations and warranted further study.

The host model used for the current study is based on the Caltech (CIT) Airshed Model. This parallel-code version of the model is under continuous development at the University of California, Irvine, in

collaboration with researchers from the California Institute of Technology and other institutions [*McRae et al*., 1982; *McRae and Seinfeld*, 1983; *Harley et al*., 1993; *Meng et al*., 1997, 1998; *Griffin et al*., 2002b]. The model employs the new CACM chemical mechanism, consisting of 361 chemical reactions, and tracks 123 gas-phase species. Aerosol particles are modeled using an internally mixed assumption, i.e. all particles within a size bin are assumed to have the same composition. The thermodynamics module Simulating Composition of Atmospheric Particles at Equilibrium 2 (SCAPE2) is used to describe the gas-aerosol partitioning of inorganic aerosol constituents [*Kim et al.,* 1993; *Meng et al*., 1995].

Open ocean aerosol fluxes are calculated using the function of Monahan and coworkers [*Monahan et al.,* 1986] widely used in global atmospheric sea-salt aerosol models [*Gong et al.,* 1997a; *Erickson et al,* 1999]. In the littoral region, wave breaking is dominated by interaction with the sea bottom surface. Extensive, near complete, whitecap coverage can therefore develop even at very low wind speeds producing sea-salt aerosol concentrations that are 1–2 orders higher than the oceanic background. A wind-speed dependent mathematical expression, developed from studies performed on the California coast, is included in the model in order to simulate the flux of surf-zone aerosol to the coastal boundary layer [*De Leeuw et al.,* 2000].

Twelve gas-phase species and 83 gas-phase reactions have been added to the host model in order to represent the chemistry of photochemically active chlorine-containing gases derived from sea-salt particles. The gas-phase chlorine chemistry mechanism in this study represents the most detailed compilation of its kind ever implemented into an urban photochemical model. There are limited chamber data at present to test chlorine radical initiated VOC oxidation mechanisms [*California Air Resources Board*, 1999] and significant uncertainties arise during mechanism development. Nonetheless, for the purpose of this study, the mechanism is more than satisfactory to provide a first estimate of the impact of sea-salt derived chlorine chemistry in urban coastal regions.

Heterogeneous/multiphase chemical reactions considered key processes leading to reactive chlorine concentrations in urban coastal regions are incorporated in to the model. Included is a mechanism of chlorine formation initiated by the heterogeneous reaction of the hydroxyl radical with chloride ions at the

gas-liquid interface of deliquesced salt particles [*Oum et al.,* 1998; *Knipping et al.*, 2000; *Knipping and Dabdub,* 2002]. The multiphase reactions of dinitrogen pentoxide (N_2O_5) [*Fenter et al.,* 1996; *Behnke et al.*, 1997; *Schweitzer et al.,* 1998; *Gebel and Finlayson-Pitts,* 2001], and chlorine nitrate ($ClONO_2$) [*Caloz et al.,* 1996; *Wincel et al.,* 1997] with sea-salt particles are also included in the model mechanism. The reaction of the nitrate radical on sea-salt particles is added in a sensitivity run for insight on the effect of a potential nighttime mechanism for chlorine release from sea-salt particles.

Included in the SCAPE2 thermodynamic module [*Kim et al.,* 1993*; Meng and Seinfeld,* 1995] of the CIT Airshed Model are several heterogeneous/multiphase equilibrium reactions that account for HCl displacement by less-volatile stronger acids, such as nitric and sulfuric acid. However, apart from these equilibrium expressions, aqueous-phase chemical reactions are absent from the computations. Heterogeneous/multiphase chemistry is treated excluding reactions occurring in the bulk of the aqueous component of atmospheric aerosol particles

Air quality simulations of conditions of September 8 – 9, 1993 are presented in this study. Meteorological data for this episode were supplied by the South Coast Air Quality Management District (SCAQMD) [*Griffin et al*., 2002b]. These parameters include relative humidity, temperature, wind, ultraviolet solar radiation, total solar radiation, and mixing height. Gas and particulate emissions inventory for this episode were supplied directly by the South Coast Air Quality Management District [*Griffin et al*., 2002b], except for sea-salt particle emissions that were calculated using either the open ocean or surf-zone sea-salt particle source functions described earlier.

Five modeling simulation were performed, as summarized in Table 8. A Base Case simulation served a benchmark to evaluate the other four test simulations. Results of the Base Case show ozone concentrations increasing throughout the eastern region of the domain as the day progresses. These results manifest the complexity of the air quality episode selected for this study. Low ozone concentrations in the center region of the domain are attributed to excess NO_x titration of ozone by the model. Overly high nighttime concentrations of ozone in the northeastern region of the domain result from difficulties

encountered by numerical models in simulating physical phenomena at the boundaries and in estimating eddy diffusivities at low-winds speeds such as those that characterized the selected air-quality episode.

Table 8: Summary of simulation scenarios

Simulation Name	Description	Comments on Cl_2 Values	Influence on O_3 Concentrations
Base Case	Simulation *without* gas-phase chlorine chemistry or heterogeneous/ multiphase chemistry on sea-salt particles, except for acid displacement reactions.	*Simulation used as a benchmark to evaluate the four test simulations.*	
Case Cl Chem	Simulation *including* heterogeneous/multiphase reactions of OH, N_2O_5 and $ClONO_2$ on sea-salt particles and full mechanism of gas-phase chlorine chemistry.	Nighttime to pre-dawn Cl_2 concentration peaks at ~12 ppt	Ozone levels increase by up to ~10 ppb compared to 'Base Case' simulation. (See Figure 11). Domain peak ozone increases by ~4 ppb. Station-wide peak ozone increases by ~2 ppb.
Case Cl Chem & NO_3 Reaction	Same as 'Case Cl-Chem' with additional reaction of the nitrate radical on sea-salt particles.	Nighttime to pre-dawn peaks Cl_2 concentration peaks at ~600 ppt; during daytime, $[Cl_2]$ and [Cl] appear fairly similar to 'Case Cl Chem' simulation	Ozone differences increase slightly in most regions compared to 'Case Cl Chem' simulation. Peak ozone similar to 'Case Cl Chem.'
$[Cl_2]$ = 150 ppt	Same as 'Case Cl-Chem' but prescribing a constant Cl_2 concentration of 150 ppt throughout the model domain.	Simulation used in order to gain insight on potential effects of added/unknown anthropogenic sources of photochemically active chlorine species.	Ozone concentrations are increased significantly throughout the domain during daytime.
$[Cl_2]$ = 1500 ppt	Same as 'Case Cl-Chem' but prescribing a constant Cl_2 concentration of 1500 ppt throughout the model domain.	Extreme simulation to further test the chemical mechanism.	Ozone concentrations are increased throughout a large portion of the domain during the entire day. New ozone peaks develop. Temporal and spatial dynamics affected altogether. Some regions exhibit ozone decreases.

Modeling results show that twenty-four hour average PM_{10} and $PM_{2.5}$ sodium mass observations are adequately reproduced by the model. Sea-salt concentrations are dominated by the surf-zone production of sea-spray; the open-ocean contribution to coastal sea-salt aerosol concentrations is negligible. Although some sea-salt particles do travel for several tens of kilometers inland, concentrations are quite low beyond coastal regions. Chloride-to-sodium ratios calculated throughout the basin exhibit chloride deficits. As expected, this effect is due primarily to hydrochloric acid displacement by less-volatile

stronger acids. The newly added heterogeneous/multiphase chemical reactions do not significantly affect the rate of acid displacement nor do they enhance aerosol nitrate formation

The maximum 1-hour average [Cl_2] predicted by the 'Case Cl Chem' simulation is 12 ppt, predicted both in the late evening and at pre-dawn. Whereas *Spicer et al.* [1998] coworkers measured Cl_2 concentrations around 150 ppt in their field campaign, and the mist chamber measurements of *Keene et al.* [1993] suggest Cl_2 concentrations up to 127 ppt, the model predicts concentrations that are an order of magnitude below the observed values. Nonetheless, these predictions represent an increase by a factor of 30 in the ability to reproduce Cl_2 values when compared to the maximum Cl_2 concentrations predicted by the box model of Spicer and coworkers.

The results of the 'Case Cl Chem' simulation show that sea-salt chemistry, even when Cl_2 levels are under-predicted, can contribute in a non-negligible fashion to ozone concentrations. The results of the 'Case Cl Chem' simulation suggest that inclusion of sea-salt derived chlorine chemistry in photochemical models may increase morning ozone predictions by as much as ~12 ppb in coastal regions and by ~ 4 ppb to the peak domain ozone in the afternoon. Although the influence dissipates in later hours, the fraction of the basin affected by the chlorine chemistry increases due to the influence of various physicochemical processes, with transport being the dominant process. The peak ozone concentrations at most monitoring sites increases by 2 – 4 ppb and even higher ozone increases, up to 7 ppb, are predicted at other times not coinciding with the peak. Overall, ozone exposure is increased throughout the domain.

Addition of a nighttime mechanism of chlorine formation, as shown by the 'Case Cl Chem & NO_3 Reaction' simulation, increases Cl_2 predictions to values more consistent with the measurements of *Spicer et al.* [1998] and *Keene et al.* [1993]. In a few small areas, the predicted values (~600 ppb) actually exceed by a factor of 4 those measured by the field campaigns, but good agreement is obtained in general. The increase of Cl_2 does not endure past the dawn, when photolysis of both NO_3 and Cl_2 bring the molecular chlorine concentration down to similar levels as the 'Case Cl Chem' simulation. Consequently, the impact of adding the nitrate radical reaction on the sea-salt particles on ozone concentrations is not as marked as the impact witnessed on pre-dawn Cl_2 concentrations. Morning differences between ozone

predictions in this scenario versus the 'Base Case' are increased by < 2 ppb in coastal regions when compared to those illustrated on Figure 11 for the 'Case Cl Chem' simulation, with the effect lessening throughout the day. Overall, the same general behavior in ozone formation is exhibited by the 'Case Cl Chem & NO_3 Reaction' simulation as the 'Case Cl Chem' simulation. The nature of the true nighttime chemistry leading to Cl_2 formation is still uncertain, with some researchers suggesting a ferric-ion catalyzed reaction of chloride with background ozone [*Sadanaga et al.,* 2001] in lieu of a nitrate-radical

6. Recommendations

This study demonstrates that chlorine chemistry may impact the prediction of ozone concentrations by air-quality models. However there are still a fair amount of uncertainties that require additional investigation. Following is a list of recommendations for future research.

- Although sea-spray is the most evident source of chlorine in a coastal region, anthropogenic sources of chlorine may have a similar or greater impact on ozone formation. Researchers in Texas identified cooling towers, swimming pools and industrial activity as principal sources of photochemically active inorganic chlorine in the atmosphere [*Tanaka and Allen*, 2001]. An emissions inventory for anthropogenic chlorine sources should be developed for the South Coast Air Basin.
- The gas-phase chlorine chemistry mechanism presented in this study is an initial step in the development of a comprehensive chlorine chemistry mechanism for urban photochemical modeling. This mechanism should be continually reviewed and validated by chamber studies. For instance, reactions of the chlorine radical with other organics (e.g. methyl glyoxal, methyl vinyl ketone, methacrolein and phenols) may be added.
- Measurements of species that serve as chlorine chemistry markers should be performed to validate and complement future modeling studies [*Wang and Finlayson-Pitts*, 2001].
- Heterogeneous/multiphase reactions on sea-salt particles should continue to be investigated. It is important that these studies not only address the implications to atmospheric processes, but also provide or suggest parameterizations that may be used by the modeling community.
- The treatment of heterogeneous/multiphase reactions should be refined in future modeling studies. In addition, other reactions, such as the hydrolysis of N_2O_5 and $ClONO_2$, should also be added to the chemical mechanism.
- Future modeling studies should relax the internally-mixed aerosol assumption and, at the very least, model an external mixture of marine aerosol particles and other regional aerosol particles.

Once photochemical models simulate an external mixture of particles, aqueous-phase chemistry within the marine aerosol constituent should be incorporated in a manner similar to current marine boundary layer and cloud models. These simple statements do not reflect the complexity of this task which requires extensive study and careful planning before implementation.

- Other air-quality episodes should be modeled, including simulations using future-year estimated emissions. The episode chosen for this study presents several challenges with respect to the correct modeling of transport processes in the atmosphere. Although files containing the flux of Cl_2 and $ClNO_2$ from sea-salt particles are included in Appendix B, these fluxes are only representative of the particular episode chosen for this study.
- Studies should be performed to determine the sensitivity of the model to in certain parameters. For example, the model response to variation in the parameters in the sea-salt source functions should be investigated. Sensitivity studies will also provide more insight on which parameters most influence chlorine atom concentrations.
- The reactions of organochlorine species were assumed negligible for the purpose of urban regional modeling in this study. The appropriateness of this assumption should be reevaluated once other greater uncertainties have been addressed.

References:

Andreas, E. L., Time constants for the evolution of sea spray droplets, *Tellus, 42B,* 481-497, 1990.

Andreas, E. L., Sea spray and the turbulent air-sea heat fluxes, *J. Geophys. Res., 97,* 11429-11441, 1992.

Andreas, E. L., A new sea spray generation function for wind speeds up to 32 m s^{-1}, *J. Phys. Oceanogr., 28,* 2175-2184, 1998.

Andreas, E. L., J. B. Edson, E. C. Monahan, M. P. Rouault, and S. T. Smith, The spray contribution to net evaporation to net evaporation from the sea: A review of recent progress, *Boundary-Layer Meteorolog., 72,* 3-52, 1995.

Andreas, E. L., M. J. Pattison, and S. E. Belcher, "Production rates of sea-spray droplets" by M. J. Pattison and S. E. Belcher: Clarification and elaboration, *J. Geophys. Res., 106,* 7157-7161, 2001.

Atkinson, R., Gas-phase chemistry of volatile organic compounds: 1. Alkanes and alkenes, *J. Phys. Chem. Ref. Data, 26,* 215-290, 1997.

Atkinson, R., D. L. Baulch, R. A. Cox, R. F. Hampson, Jr., J. A. Kerr, M. J. Rossi, and J. Troe, Evaluated kinetic and photochemical data for atmospheric chemistry: Supplement V, *J. Phys. Chem. Ref. Data, 26,* 521-549, 1997a.

Atkinson, R., D. L. Baulch, R. A. Cox, R. F. Hampson, Jr., J. A. Kerr, M. J. Rossi, and J. Troe, Evaluated kinetic and photochemical data for atmospheric chemistry: Supplement VI, *J. Phys. Chem. Ref. Data, 26,* 1329-1499, 1997b.

Atkinson, R., D. L. Baulch, R. A. Cox, R. F. Hampson, Jr., J. A. Kerr, M. J. Rossi, and J. Troe, Evaluated kinetic and photochemical data for atmospheric chemistry, organic species: Supplement VII, *J. Phys. Chem. Ref. Data, 28,* 191-365, 1999.

Atkinson, R., D. L. Baulch, R. A. Cox, R. F. Hampson, Jr., J. A. Kerr, M. J. Rossi, and J. Troe, Evaluated kinetic and photochemical data for atmospheric chemistry: Supplement VIII, Halogen species evaluation for atmospheric chemistry, *J. Phys. Chem. Ref. Data, 29,* 167-266, 2000.

Behnke, W., V. Scheer and C. Zetzsch, Production of $BrNO_2$, Br_2 and $ClNO_2$ from the reaction between sea spray aerosol and N_2O_5, *J. Aerosol Sci., 25,* S277-S278, 1994.

Behnke, W., C. George, V. Scheer, and C. Zetzsch, Production and decay of $ClNO_2$ from the reaction of gaseous N_2O_5 with NaCl solution: Bulk and aerosol experiments, *J. Geophys. Res., 102,* 3795-3804, 1997.

Bey, I., B. Aumont, and G. Toupance, The nighttime production of OH radicals in the(h)unin(t)4(i)4(n)-1.4en(t)4actupu rph0 ReD. ettW.,246,

California Energy Commission, Database of California Power Plants, <available from: http://www.energy.ca.gov/database/index.html#powerplants>, State of California, 2001.

Caloz, F., F. F. Fenter, and M. J. Rossi, Heterogeneous kinetics of the uptake of $ClONO_2$ on NaCl and KBr, *J. Phys. Chem, 100,* 7494-7501, 1996.

Canosa-Mas, C. E., H. R. Hutton-Squire, M. D. King, D. J. Stewart, K. C. Thompson and R. P. Wayne, Laboratory kinetic studies of the reactions of Cl atoms with species of biogenic origin, Δ^3-carene, isoprene, methacrolein and methyl vinyl ketone, *J. Atmos. Chem.,* 163-170, 1999.

Carter, W. P. L., D. Luo, and I. L. Malkina, Environmental chamber studies for development of an updated photochemical mechanism for VOC reactivity assessment, Draft final report to California Air Resources Board Contract 92-345, Coordinating Research Council Project M-9, and National Renewable Energy Laboratory Contract ZF-2-12252-07, <available from http://pah.cert.ucr.edu/~carter/saprc97.htm>, 1997a.

Carter, W. P. L., D. Luo, and I. L. Malkina, Investigation of the atmospheric reactions of chloropicrin, *Atmos. Environ, 31,* 1425-1439, 1997b

Chang, S., P. Tanaka, E. McDonald-Buller, D. T. Allen, Emission inventory for atomic chlorine precursors in Southeast Texas, <available from: http://www.tnrcc.state.tx.us/air/aqp/airquality_contracts.html>, Texas Natural Resource Conservation Commission, 2001.

Chang, S., E. McDonald-Buller, Y. Kimura, M. M. Russell, P. L. Tanaka, D. T. Allen, Spatial and temporal impacts of chlorine chemistry on ozone formation in Southeastern Texas, <available from: http://www.tnrcc.state.tx.us/air/aqp/airquality_contracts.html>, Texas Natural Resource Conservation Commission, 2002.

Coquet, S., and P. Ariya, Kinetics of the gas-phase reactions of Cl atom with selected $C_2 - C_5$ unsaturated hydrocarbons at $283 < T < 323$ K, *Int. J. Chem. Kinet., 32,* 478-484, 2000.

De Leeuw, G., F. P. Neele, M. Hill, M. H. Smith, and E. Vignati, Production of sea spray aerosol in the surf zone, *J. Geophys. Res., 105,* 29397-29409, 2000.

DeCosmo, J., K. B. Kastsaros, S. D. Smith, R. J. Anderson, W. A. Oost, K. Bumke, and H. Chadwick, Air-sea exchange of water vapor and sensible heat: The Humidity Exchange Over the Sea (HEXOS) results, *J. Geophys. Res., 101,* 12001-12016, 1996.

DeMore, W. B., S. P. Sander, D. M. Golden, R. F. Hampson, M. J. Kurylo, C. J. Howard, A. R. Ravishankara, C. E. Kolb and M. J. Molina, *Chemical Kinetics and Photochemical Data for Use in Stratospheric Modeling, Rep. 97-4*, Jet Propulsion Laboratory, Pasadena, CA, 1997.

Donaldson, D. J., A. R. Ravishankara and D. R. Hanson, Detailed Study of HOCl + HCl → Cl_2 + H2O in Sulfuric Acid, *J. Phys. Chem. A, 101,* 4717-4725, 1997.

Edson, J. B. and C. W. Fairall, Spray droplet modeling 1. Lagrangian model simulation of the turbulent transport of evaporating droplets, *J. Geophys. Res., 99,* 25295-25311, 1994.

Erickson, D. J., C. Seuzaret, W. C. Keene, and S. L. Gong, A general circulation model based calculation of HCl and ClNO2 production from sea-salt dechlorination: Reactive Chlorine Emissions Inventory, *J. Geophys. Res., 104,* 8347-8372, 1999.

Faloona, I., D. Tan, W. Brune, J. Hurst, D. Barket, Jr., T. L. Couch, P. Shepson, E. Apel, D. Riemer, T. Thornberry, M. A. Carroll, S. Sillman, G. J. Keeler, J. Sagady, D. Hooper, and K. Patterson, Nighttime observations of anomalously high levels of hydroxyl radicals above a deciduous forest canopy, *J. Geophys. Res., 106,* 24315-24333, 2001.

Fantechi, G., N. R. Jensen, O. Saastad, J. Hjorth, and J. Peeters, Reactions of Cl atoms with selected VOCs: Kinetics, products and mechanisms, *J. Atmos. Chem., 31,* 247-267, 1998.

Fenter, F. F., F. Caloz, and M. J. Rossi, Heterogeneous kinetics of N_2O_5 uptake on salt, with a systematic study of the role of surface presentation (for N_2O_5 and HNO_3), *J. Phys. Chem., 100,* 1008-1019, 1996.

Finlayson-Pitts, B. J., Chlorine atoms as a potential tropospheric oxidant in the marine boundary layer, *Res. Chem. Intermediat., 19,* 235-249, 1993.

Finlayson-Pitts, B. J., C. J. Keoshian, B. Buehler, A. A. Ezell, Kinetics of Reaction of Chlorine Atom with Some Biogenic Organics, *Int. J. Chem. Kinet., 31,* 491-499, 1999.

Finlayson-Pitts, B. J. and J.C. Hemminger, Physical chemistry of airborne sea-salt particles and their components, *J. Phys. Chem. A, 104,* 11463-11477, 2000.

Finlayson-Pitts, B. J. and J. N. Pitts Jr., Tropospheric Air Pollution: Ozone, Airborne Toxics, Polycyclic Aromatic Hydrocarbons, and Particles, *Science, 276,* 1045-1052, 1997.

Finlayson-Pitts, B. J. and J. N. Pitts, Jr., *Chemistry of the Upper and Lower Atmosphere: Theory, Experiments and Applications*, Academic Press, San Diego, 2000.

Fitzgerald, J. W., Marine aerosols: A review, *Atmos. Chem., 25A,* 533-545, 1991.

Fraser, M. P., M. J. Kleeman, J. J. Schauer, and G. R. Cass, Modeling the atmospheric concentrations of individual gas-phase and particle-phase organic compounds, *Environ. Sci. Technol*., *34*, 1302-1312, 2000.

Fraser, M. P., G. R. Cass, and B. R. T. Simoneit, Gas-phase and particle-phase organic compounds emitted from motor vehicle traffic in a Los Angeles roadway tunnel, *Environ. Sci. Technol*., *32*, 2051-2060, 1998.

Gard, E. E., M. J. Kleeman, D. S. Gross, L. S. Hughes, J. O. Allen, B. D. Morrical, D. P. Fergenson, T. Dienes, M. E. Galli, R. J. Johnson, G. R. Cass, K. A. Prather, Direct observation of heterogeneous chemistry in the atmosphere, *Science, 279,* 1184-1187, 1998.

Gebel, M. E., and B. J. Finlayson-Pitts, Uptake and reaction of $ClONO_2$ on NaCl and synthetic sea salt, *J. Phys. Chem. A, 105*, 5178-5187, 2001.

Gershenzon, M. Y., S. Ilin, N. G. Fedotov, Y. M. Gershenzon, E. V. Aparina, and V. V. Zelenov, The mechanism of reactive NO_3 uptake on Dry NaX (X=Cl, Br), *J. Atmos. Chem., 34,* 119-135, 1999.

Gharib, S. and G.R. Cass, Ammonia emissions in the South Coast Air Basin, open file report 84-2, Environmental Quality Laboratory: California Institute of Technology, Pasadena, CA, 1984.

Gong, S. L., L. A. Barrie, and J.-P. Blanchet, Modeling sea-salt aerosols in the atmosphere 1. Model development, *J. Geophys. Res., 102,* 3805-3818, 1997a.

Gong, S. L., L. A. Barrie, J. M. Prospero, D. L. Savoie, G. P. Ayers, J.-P. Blanchet, and L. Spacek, Modeling sea-salt aerosols in the atmosphere 2. Atmospheric concentrations and fluxes, *J. Geophys. Res., 102,* 3819-3830, 1997b.

Griffin, R. J., D. Dabdub, and J. H. Seinfeld, Secondary organic aerosol: I. Atmospheric chemical mechanism for production of molecular constituents, *J. Geophys. Res., in press,* 2002a.

Harris County, Texas, Pollution Control Division, Harris Country Toxic Release Inventory, <available via: http://www.hd.co.harris.tx.us/pcd/>, Harris County Public Health & Environmental Services, 2001.

Hanson, D. R., Surface-Specific Reactions on Liquids, *J. Phys. Chem. B, 101*, 4998-5001, 1997.

Hanson, D. R., A. R. Ravishankara and S. Solomon, Heterogeneous reactions in sulfuric acid aerosols: A framework for model calculations, *J. Geophys. Res., 99*, 3615-3629, 1994.

Harley, R. A., A. G. Russell, G. J. McRae, G. R. Cass, and J. H. Seinfeld, Photochemical modeling of the Southern California Air Quality Study, *Environ. Sci. Technol*., *27*, 378-388, 1993.

Hermann, H., B. Ervens, H.-W. Jacobi, R. Wolke, P. Nowacki, and R. Zellner, CAPRAM 2.3: A chemical aqueous phase radical mechanism for tropospheric chemistry, *J. Atmos. Chem., 36,* 231-284, 2000.

Hughes, L. S., J. O. Allen, P. Bhave, M. J. Kleeman, G. R. Cass, D.-Y. Liu, P. Fergenson, B. D. Morrical, and K. A. Prather, Evolution of atmospheric particles along trajectories crossing the Los Angeles basin, *Environ. Sci. Technol., 34,* 3058-3068, 2000.

IUPAC, Subcommittee for Gas Kinetic Data Evaluation: Heterogeneous Data Sheets (Reactive), <available from: http://www.iupac-kinetic.ch.cam.ac.uk/r_het.php>, International Union of Pure and Applied Chemistry, 2000.

Jacob, D. J., Heterogeneous chemistry and tropospheric ozone, *Atmos. Environ., 34,* 2131-2159, 2000.

Jenkin, M. E., S. M. Saunders, and M. J. Pilling, The tropospheric degradation of volatile organic compounds: a protocol for mechanism development, *Atmos. Environ., 31,* 81-104, 1997.

John, W., S.M. Wall, J.L. Ondo, and W. Winklmayr, *Acidic aerosol size distributions during SCAQS*: Report to the California Air Resources Board under Contract A6-112-39, 1990.

Keene, W. C., A. A. P. Pszenny, D. J. Jacob, R. A. Duce, J. N. Galloway, J. J. Schultz-Tokos, H. Sievering, and J. F. Boatman, The geochemical cycling of reactive chlorine through the marine troposphere, *Global Biogeochem. Cycles, 4,*407-430, 1990.

Keene, W. C., J. R. Maben, A. A. Pszenny, and J. N. Galloway, Measurement technique for inorganic chlorine gases in the marine boundary layer, *Environ. Sci. Technol., 27,* 866-874, 1993.

Keene, W. C., R. Sander, A. A. P. Pszenny, R. Vogt, P. J. Crutzen, and J. N. Galloway, Aerosol pH in the marine boundary layer: A review and model evaluation, *J. Aerosol Sci., 29,* 339-359, 1998.

Keene, W. C., M. A. K. Khalil, D. J. Erickson, A. McCulloch, T. E. Graedel, J. M. Lobert, M. L. Aucott, S. L. Gong, D. B. Harper, G. Kleiman, P. Midgley, R. M. Moore, C. Seuzaret, W. T. Sturges, C. M. Berkowitz, V. Koropalov, L. A. Barrie, and Y. F. Li, Composite global emissions of reactive chlorine from anthropogenic and natural sources: Reactive Chlorine Emissions Inventory, *J. Geophys. Res., 104,* 8429-8440, 1999.

Khalil, M. A. K., R. M. Moore, D. B. Harper, J. M. Lobert, D. J. Erickson, V. Koropalov, W. T. Sturges, and W. C. Keene, Natural emissions of chlorine containing gases: Reaction Chlorine Emissions Inventory, *J. Geophys. Res., 104,* 8333-8346, 1999.

Kim, Y. P., J. H. Seinfeld, and P. Saxena, Atmospheric gas-aerosol equilibrium I. Thermodynamic module, *Aerosol Sci. Technol., 19,* 157-181, 1993.

Knipping, E. M., M. J. Lakin, K. L. Foster, P. Jungwirth, D. J. Tobias, R. B. Gerber, D. Dabdub, and B. J. Finlayson-Pitts, Experiments and simulations of ion-enhanced interfacial chemistry on aqueous NaCl aerosols, *Science, 288,* 301-306, 2000.

Knipping, E. M. and D. Dabdub, Modeling study of Cl_2 formation from aqueous NaCl particles: Evidence for interfacial reactions and importance of Cl_2 decomposition in alkaline solution. *J. Geophys. Res., in review,* 2002.

Maricq, M. M., J. J. Szente, E. W. Kaiser and J. C. Shi , Reaction of chlorine atoms with methylperoxy and ethylperoxy radicals, *J. Phys. Chem, 98,* 2083-2089, 1994.

McRae, G. J., and J. H. Seinfeld, Development of a second-generation mathematical model for urban air pollution 2. Evaluation of model performance, *Atmos. Environ*., *17*, 501-522, 1983.

McRae, G. J., W. R. Goodin, and J.H. Seinfeld, Development of a second-generation mathematical model for urban air pollution 1. Model formulation, *Atmos. Environ*., *16*, 679-696, 1982.

Meng, Z., D. Dabdub, and J. H. Seinfeld, Chemical coupling between atmospheric ozone and particulate matter, *Science, 277,* 166-119, 1997.

Meng, Z., D. Dabdub, and J. H. Seinfeld, Size-resolved and chemically resolved model of aerosol dynamics, *J. Geophys. Res., 103,* 3419-3435, 1998.

Meng, Z., J.H. Seinfeld, P. Saxena, and Y.P. Kim, Atmospheric gas-aerosol equilibrium IV Thermodynamics of carbonates, *Aerosol Sci. Technol*., *23*, 131-154, 1995.

Millero, F. J., *Chemical Oceanography, Second Edition*, CRC Press, Boca Raton, Florida, 1996.

Moldanova, J. and E. Ljungstrom, Sea-salt aerosol chemistry in coastal areas: A model study, *J. Geophys. Res., 106,* 1271-1296, 2001.

Monahan, E. C., D. E. Spiel, and K. L. Davidson, A model of marine aerosol generation via whitecaps and wave disruption, in *Oceanic Whitecaps,* E. C. Monaham and G. Mac Niocaill (eds.), D. Riedel Publishing Co., 1986.

Notario, A., G. Le Bras, and A. Mellouki, Kinetics of Cl atoms reactions with butadienes including isoprene, *Chem. Phys. Lett., 281,* 421-425, 1997.

Notario, A., A. Mellouki, G. Le Bras, Rate constants for the gas-phase reactions of chlorine atoms with a series of ketones, *Int. J. Chem. Kinet., 32,* 62-66, 2000a.

Notario, A., A. Mellouki, G. Le Bras, Rate constants for the gas-phase reactions of chlorine atoms with a series of ethers, *Int. J. Chem. Kinet., 32,* 105-110, 2000b.

O'Dowd, C. D., and M. H. Smith, Physicochemical properties of aerosols over the Northeast Atlantic: Evidence for wind-speed-related submicron sea-salt aerosol production, *J. Geophys. Res., 98,* 1137-1149, 1993.

Oum, K. W., M. J. Lakin, D. O. DeHaan, T. Brauers, and B. J. Finlayson-Pitts, Formation of molecular chlorine from the photolysis of ozone and aqueous sea-salt particles, *Science, 279,* 74-77, 1998.

Pattison, M. J. and S. E. Belcher, Production rates of sea-spray droplets, *J. Geophys. Res., 104,* 18397-18407, 1999.

Ragains, M. L. and B. J. Finlayson-Pitts, Kinetics and mechanism of the reaction of Cl atoms with 2-methyl-1,3-butadiene (Isoprene) at 298 K, *J. Phys. Chem. A, 101,* 1509-1517, 1997.

Pierson, W. R., A. W. Gertler, and R. L. Bradow, Comparison of the SCAQS tunnel study with other on-road vehicle emission data, *J. Air Waste Manage. Assoc*., *40*, 1495-1504, 1990.

Pilgrim, J. S., A. McIlroy, and C. A. Taatjes, Kinetics of Cl Atom Reactions with Methane, Ethane, and Propane from 292 to 800 K, *J. Phys. Chem. A, 101,* 1873-1880, 1997.

Pun, B. K., R. J. Griffin, C. Seigneur, and J. H. Seinfeld, Secondary organic aerosol: II. Thermodynamic model for gas/particle partitioning of molecular constituents, *J. Geophys. Res*., *in press*, 2002.

Pszenny, A. A. P., W.C. Keene, D. J. Jacob, S. Fan, J. R. Maben, M. P. Zetwo, M. Springer-Young and J. N. Galloway, Evidence of Chlorine Gases Other than Hydrogen Chloride in Marine Surface Air, *Geophys. Res. Lett., 20*, 699-702, 1993.

Reid, J. S, H. H. Jonsson, M. H. Smith, and A. Smirnov, Evolution of the vertical profile and flux of large sea-salt particles in a coastal zone, *J. Geophys. Res., 106,* 12039-12053, 2001.

Reynolds, S., Utah Division of Air Quality Planning Brach: Effects of Chlorine on Ozone Formation, <available from http://www.deq.state.ut.us/EQAIR/PLANNING/Chlorine.htm>, State of Utah, 2001.

Robinson, R. A., and R. J. Stokes, *Electrolyte Solutions*, 2nd ed., Butterworths, London, 1965.

Robinson, G. N., D. R. Worsnop, J. T. Jayne, C. E. Kolb, P. Davidovits, Heterogeneous uptake of $ClONO_2$ and N_2O_5 by sulfuric acid solution, *J. Geophys. Res., 102,* 3583-3601, 1997.

Rudich, Y., R. K. Talukdar and A. R. Ravishankara, Reactive uptake of NO_3 on pure water and ionic solutions, *J. Geophys. Res, 101, 21023-21031,* 1996.

Ravishankara, A. R., Heterogeneous and Multiphase Chemistry in the Troposphere, *Science, 276*, 1058-1065, 1997.

Sadanada, Y., Hirokawa, J. and H. Akimoto, Formation of molecular chlorine in dark condition: Heterogeneous reaction of ozone with sea-salt in presence of ferric ion, *Geophys. Res. Lett., 28 ,* 4433- 4436, 2001.

Sander, R. and P. J. Crutzen, Model study indicating halogen activation and ozone destruction in polluted air masses transported to the sea, *J. Geophys. Res., 101,* 9121-9138, 1996.

Sander, S. P., R. R. Friedl, W. B. DeMore, D. M. Golden, M. J. Kurylo, R. F. Hampson, R. E. Huie, G. K. Moortgat, A. R. Ravishankara, C. E. Kolb and M. J. Molina, *Chemical Kinetics and Photochemical Data for Use in Stratospheric Modeling, Rep. 00-3*, Jet Propulsion Laboratory, Pasadena, CA, 2000.

Schwartz, S. E., Mass-transport Considerations Pertinent to Aqueous-phase Reactions of Gases in Liquid-water Clouds, in *Chemistry of Multiphase Atmospheric Systems, NATO ASI Series, Vol. G6* (edited by W. Jaeschke), Springer-Verlag, Berlin Heidelberg, 1986.

Schweitzer, F., P. Mirabel, and C. George, Multiphase chemistry of N_2O_5, $ClNO_2$ and $BrNO_2$, *J. Phys. Chem. A., 102,* 3942-3952, 1998.

Seinfeld, J. H. and S. Pandis, *Atmospheric Chemistry and Physics: From Air Pollution to Climate Change*, Wiley, New York, 1998.

Seisel S., B. Fluckiger, F. Caloz and M. J. Rossi, Heterogeneous reactivity of the nitrate radical : reactions on halogen salt at ambient temperature and on ice in the presence of HX (X = Cl, Br, I) at 190 K, Phys. Chem. Chem. Phys., 1, 2257-2266, 1999.

Smith, M. H., P. M. Park, and I. E. Consterdine, Marine aerosol concentrations and estimated fluxes over the sea, *Q. J. R. Meterol. Soc., 119,* 809-824, 1993.

Spicer, C. W., E. G. Chapman, B. J. Finlayson-Pitts, R. A. Plasteridge, J. M. Hubbe, J. D. Fast, and C. M. Berkowitz, Unexpectedly high concentrations of molecular chlorine in coastal air, *Nature, 394,* 353-356, 1998.

Spiel, D. E., The sizes of the jet drops produced by air bubbles bursting on sea- and fresh-water surfaces, *Tellus, 46B,* 325-338, 1994a.

Spiel, D. E., The number and size of jet drops produced by air bubbles bursting on a fresh water surface, *J. Geophys. Res., 99,* 10289-10296, 1994b.

Spiel, D. E., On the births of jet drops from bubbles bursting on water surfaces, *J. Geophys. Res., 100,* 4995-5006, 1995.

Spiel, D. E., A hypothesis concerning the peak in film drop production as a function of size, *J. Geophys. Res., 102,* 1153-1161, 1997.

Spiel, D. E., On the births of film drops from bubbles bursting on seawater surfaces, *J. Geophys. Res., 103,* 24907-24918, 1998.

Stockwell, W. R., F. Kirchner, M. Kuhn, and S. Seefeld, A new mechanism for regional atmospheric chemistry modeling, *J. Geophys. Res., 102,* 25847-25879, 1997.

Stramska, M., R. Marks, and E. C. Monahan, Bubble-mediated aerosol production as a consequence of wave breaking in supersaturated seawater, *J. Geophys. Res., 95,* 18281-18288, 1990.

Stutz, J., M. J. Ezell, A. A. Ezell, and B. J. Finlayson-Pitts, Rate constants and kinetic isotope effects in the reactions of atomic chlorine with *n*-butane and simple alkenes at room temperature, *J. Phys. Chem. A, 102,* 8510-8519, 1998.

Suh, I., and R. Zhang, Kinetic studies of isoprene reactions initiated by chlorine atom, *J. Phys. Chem. A, 104,* 6590-6596, 2000.

Tanaka, P. L., S. Oldfield, J. D. Neece, C. B. Mullins, and D. T. Allen, Anthropogenic sources of chlorine and ozone formation in urban atmospheres, *Environ. Sci. Technol., 34,* 4470-4473, 2000.

Tanaka, P. L. and D. T. Allen, Incorporation of chlorine reactions into the Carbon Bond IV Mechanism: Mechanism updates and preliminary performance evaluation, <available from: http://www.tnrcc.state.tx.us/air/aqp/airquality_contracts.html>, Texas Natural Resource Conservation Commission, 2001.

Toyota, K., M. Takahashi, and H. Akimoto, Modeling multi-phase halogen chemistry in the marine boundary layer with size-segregated aerosol module: Implications for quasi-size-dependent approach, *Geophys. Res. Lett., 28,* 2899-2902, 2001.

Vignati, E., G. De Leeuw, R. Berkowitz, Modeling coastal aerosol transport and effects of surf-produced aerosols on processes in the marine atmospheric boundary layer, *J. Geophys. Res., 106,* 20225-20238, 2001.

Vogt, R., P. J. Crutzen, and R. Sander, A mechanism for halogen release from sea-salt aerosol in the marine boundary layer, *Nature, 383,* 327-330, 1996.

Wang, W., and B. J. Finlayson-Pitts, Unique markers of chlorine atoms chemistry in coastal urban areas: The reaction with 1,3-butadiene in air at room temperature, *J. Geophys. Res., 106,* 4939-4958, 2001.

Wincel, H., E. Mereand, and A. W. Castleman, Gas-phase reactions of $ClONO_2$ with $Cl^-(D_2O)_{n=0-3}$ and NO_2^-, *J. Phys. Chem. A, 101,* 8248-8254, 1997.

Winner, D. A., and G. R. Cass, Modeling the long-term frequency distribution of regional ozone concentrations, *Atmos. Environ*., *33*, 431-451, 1999.

Woolf, D. K., P. A. Bowyer, and E. C. Monahan, Discriminating between the film drops and jet drops produced by simulated whitecap, *J. Geophys. Res., 92,* 5142-5150, 1987.

Wu, J., Film drops produced by air bubbles bursting at the surface of seawater, *J. Geophys. Res., 99,* 16403-16407, 1994.

Appendix A: Gas-Phase Chlorine Chemistry Mechanism

Table A.1 below lists the species contained in the CalTech Chemical Mechanism, CACM [*Griffin et al.*, 2002a], and the species added for chlorine chemistry modeling. Table A.2 describes the gas-phase chlorine chemistry mechanism incorporated into CACM as part of this study.

Table A.1: Species included in CACM Mechanism with chlorine chemistry extensions*

NO	NITRIC OXIDE
NO2	NITROGEN DIOXIDE
O3	OZONE
HONO	NITROUS ACID
HNO3	NITRIC ACID
HNO4	PERNITRIC ACID
N2O5	NITROGEN PENTOXIDE
NO3	NITRATE RADICAL
HO2	HYDROPEROXY RADICAL
CO	CARBON MONOXIDE
CO2	CARBON DIOXIDE
H2O2	HYDROGEN PEROXIDE
NH3	AMMONIA
NIT	AEROSOL NITRATE
SO2	SULFUR DIOXIDE
SO3	SULFUR TRIOXIDE
OSD	O SINGLET D
O	O ATOM
OH	HYDROXYL RADICAL
H2O	WATER VAPOR
O2	OXYGEN
H2	HYDROGEN
M	THIRD BODY
HCL	HYDROCHLORIC ACID
CL	**ATOMIC CHLORINE**
CL2	**MOLECULAR CHLORINE**
CLO	**CHLORINE MONOXIDE**
HOCL	**HYPOCHLOROUS ACID**
CLNO	**NITROSYL CHLORIDE**
CLN2	**NITRYL CHLORIDE ($ClNO_2$)**
CLN5	**CHLORINE NITRATE ($ClONO_2$)**
OCLO	**CHLORINE DIOXIDE**
CLN3	**CHLORINE NITRITE (ClONO)**
FOCL	**FORMYL CHLORIDE (HCOCl)**
CLI1	**PRODUCT OF ISOP + CL REACTION: 4-CHLORO-3-METHYL-2-BUTANAL**
CLI2	**PRODUCT OF ISOP + CL REACTION: 4-CHLORO-2-METHYL-2-BUTANAL**
ETHE	ETHENE
OLEL	LUMPED ALKENES C3-C6
OLEH	LUMPED ALKENES >C6
ALKL	LUMPED ALKANES C3-C6
ALKM	LUMPED ALKANES C7-C12
ALKH	LUMPED ALKANES >C12
AROH	LUMPED AROMATICS WITH HIGH SOA Y
AROL	LUMPED AROMATICS WITH LOW SOA Y
PHEN	LUMPED OXYGENATED AROMATICS
BALD	LUMPED AROMATIC MONOALDEHYDES
ARAC	LUMPED AROMATIC MONOACIDS
ADAC	LUMPED AROMATIC DIACIDS

*Species in bold were added with chlorine chemistry mechanism

Table A.1 (cont.): Species included in CACM Mechanism with chlorine chemistry extensions*

PAH	LUMPED PAH
HCHO	FORMALDEHYDE
ALD2	LUMPED ALDEHYDES
MEK	LUMPED KETONES C3-C6
KETO	LUMPED KETONES >C6
MEOH	METHANOL
ETOH	ETHANOL
ALCH	LUMPED HIGHER ALCOHOLS
ISOP	ISOPRENE
BIOL	LUMPED MONOTERPENES WITH LOW SOA Y
BIOH	LUMPED MONOTERPENES WITH HIGH SOA Y
ACID	LUMPED ORGANIC ACIDS WITH <C6
PAN1	PEROXY PENTIONYL NITRATE
PAN2	PAN
PAN3	UNSATURATED PPN
PAN4	KETO PPN
PAN5	METHYLENE-PPN
PAN6	PAN FROM GLYOXAL
PAN7	PEROXY 3-METHYL-HEPTIONYL NITRATE
PAN8	PEROXY 2-HYDROXY-3-ISOPROPYL-6-OXO-HEPTIONYL NITRATE
PAN9	PEROXY 3-ISOPROPYL-4-HYDROXY-2-BUTENIONYL NITRATE
PN10	PAN FROM GLYOXALIC ACID
MGLY	METHYL GLYOXAL
MVK	METHYL VINYL KETONE
MCR	METHACROLEIN
MTBE	METHYL TERT-BUTYL ETHER
CH4	METHANE
RO2T	TOTAL RO2 ('SUM' OF RO21 THROUGH RO249 AND CLRO21 THROUGH CLRO24)
CLRO21	**RO2 RADICAL FROM ETHE + CL**
CLRO22	**RO2 RADICAL FROM OLEL + CL**
CLRO23	**RO2 RADICAL FROM OLEH + CL**
CLRO24	**RO2 RADICAL: *OOCH2Cl FROM REACTION OF CLRO21, CLRO22, CLRO23**
CRIEG1	**CRIEGEE INTERMEDIATE FROM RO21 + CL**
CRIEG2	**CRIEGEE INTERMEDIATE FROM RO25 + CL**
RO21	PEROXY FROM CH4 OXIDATION
RO22	HYDROXY ALKYL PEROXY <C6 FROM ETHE, ETOH, OLEL, ALCH
RO23	NITRATO ALKYL PEROXY <C6 FROM ETHE, OLEL
RO24	ALDEHYDIC ALKYL PEROXY FROM ISOP, ETHE
RO25	ALKYL PEROXY <C6 FROM MEK,ISOP, ALKL, BIOH, OLEL
RO26	ACYL RADICAL FROM ALD2 OXIDATION
RO27	OXO ALKYL PEROXY <C6 FROM ISOP, MEK
RO28	ACYL PEROXY <C6 FROM ALD2,ISOP, BIOH, MEK, KETO, BIOL
RO29	HYDROXY ALKENYL PEROXY FROM ISOP
RO210	HYDROXY ALKENYL PEROXY RADICAL FROM ISOP
RO211	NITRATO ALKENYL PEROXY FROM ISOP
RO212	NITRATO ALKENYL PEROXY RADICAL FROM ISOP
RO213	OXO ALKENYL PEROXY FROM ISOP
RO214	ALKENYL PEROXY FROM ISOP
RO215	ETHER ALKYL PEROXY FROM MTBE
RO216	OXO ALKYL PEROXY FROM KETO
RO217	AROMATIC PEROXY FROM SIDE CHAIN ABSTRACTION OF PHEN
RO218	HYDROXY ALKYL PEROXY >C6 FROM OLEH, ALKM
RO219	NITRATO ALKYL PEROXY FROM OLEH
RO220	ALKYL PEROXY >C6 FROM OLEH, ALKM
RO221	AROMATIC PEROXY FROM SIDE CHAIN ABSTRACTION OF AROL
RO222	PEROXY RADICAL FROM SIDE CHAIN ABSTRACTION OF BALD
RO223	PEROXY RADICAL FROM SIDE CHAIN ABSTRACTION OF ARAC

*Species in bold were added with chlorine chemistry mechanism

Table A.1 (cont.): Species included in CACM Mechanism with chlorine chemistry extensions

RO224	DIHYDROXY ALKYL PEROXY FROM OH ATTACK OF BIOL
RO225	HYDROXY NITRATO PEROXY FROM NO3 ATTACK OF BIOL
RO226	OXO HYDROXY ALDEHYDIC PEROXY FROM BIOL
RO227	HYDROXY ALKENYL PEROXY FROM BIOH
RO228	NITRATO ALKENYL PEROXY FROM BIOH
RO229	OXO ALKENYL PEROXY FROM BIOH
RO230	OXO ALDEHYDIC ALKENYL PEROXY FROM BIOH
RO231	AROMATIC PEROXY FROM SIDE CHAIN ABSTRACTION OF PAH
RO232	ALKYL PEROXY FROM ALKH
RO233	PEROXY FROM ADDITION OF O2 TO RAD2
RO234	PEROXY FROM ADDITION OF O2 TO RAD3
RO235	PEROXY FROM ADDITION OF O2 TO RAD4
RO236	PEROXY FROM ADDITION OF O2 TO RAD5
RO237	PEROXY FROM ADDITION OF O2 TO RAD6
RO238	PEROXY FROM ADDITION OF O2 TO RAD7
RO239	UNSATURATED ACYL PEROXY FROM ISOP
RO240	HYDROXY OXO ALKENYL PEROXY FROM BIOH
RO241	HYDROXY ALKYL PEROXY FROM ALKH
RO242	BICYCLIC PEROXY FROM BRIDGING OF RO233
RO243	BICYCLIC PEROXY FROM BRIDGING OF RO234
RO244	BICYCLIC PEROXY FROM BRIDGING OF RO235
RO245	BICYCLIC PEROXY FROM BRIDGING OF RO236
RO246	BICYCLIC PEROXY FROM BRIDGING OF RO237
RO247	BICYCLIC PEROXY FROM BRIDGING OF RO238
RO248	OXO ACYL PEROXY FROM FURTHER ALDEHYDE OXIDATION IN MGLY
RO249	HYDROXY KETO PEROXY RADICAL FROM MVK
RO250	ACYL PEROXY RADICAL FROM ALDEHYDIC H ATTACK OF MCR
RO251	HYDROXY ALDEHYDIC PEROXY RADICAL FROM OH DB ATTACK OF MCR
RO252	NITRATO ALDEHYDIC PEROXY RADICAL FROM NO3 DB ATTACK OF MCR
RO253	KETO ALDEHYDIC PEROXY RADICAL FROM MCR / O3 REACTION
RO254	ALDEHYDIC ACYL PEROXY RADICAL FROM RO253
RO255	ACYL PEROXY FORMED FROM FURTHER REACTION OF RPR1
RO256	HYDROXY OXO ACYL PEROXY FORMED FROM RPR3
RO257	HYDROXY UNSATURATED ACYL PEROXY FROM RPR8
RO258	ACID ACYL PEROXY RADICAL FROM RP16
RAD1	RADICAL FROM PHEN / NO3
RAD2	HEXADIENYL RADICAL FROM PHEN / OH
RAD3	HEXADIENYL RADICAL FROM AROL / OH
RAD4	HEXADIENYL RADICAL FROM AROH / OH
RAD5	HEXADIENYL RADICAL FROM BALD / OH
RAD6	HEXADIENYL RADICAL FROM ARAC / OH
RAD7	HEXADIENYL RADICAL FROM PAH / OH
RAD8	RADICAL FROM RPR4 / NO3
RPR1	3-METHYL HEPTANAL
RPR2	3-HYDROXY-4-METHYL-BENZALDEHYDE
RPR3	2-HYDROXY-3-ISOPROPYL-6-OXO-HEPTANAL
RPR4	2,6-DIMETHYL-4-NITRO-PHENOL
RPR5	2-NITRO-4-METHYL-BENZALDEHYDE
RPR6	1,4-DIBENZALDEHYDE
RPR7	1-FORMYL-4-CARBOXY-BENZENE
RPR8	3-ISOPROPYL-4-HYDROXY-2-BUTENAL
RPR9	4-HYDROXY-3,5-DIMETHYL-2,4-HEXADIENDIAL
RP10	2-METHYL-BUTENALIC ACID
RP11	4,5-DIMETHYL-6-OXO-2,4-HEPTADIENAL
RP12	2-METHYL-5-FORMYL-2,4-HEXADIENDIAL
RP13	2-CARBOXYL-5-METHYL-2,4-HEXADIENDIAL
RP14	2-(DIMETHYL-PROPENAL)-BENZALDEHYDE

Table A.1 (cont.): Species included in CACM Mechanism with chlorine chemistry extensions

RP15	2-FORMYL-ACETOPHENONE
RP16	GLYOXALIC ACID
RP17	4-HYDROXY-3,5-DIMETHYL-2,4-HEXADIENALIC ACID
RP18	2-METHYL-5-FORMYL-2,4-HEXADIENDIOIC ACID
RP19	2-(DIMETHYL-PROPENAL)-BENZOIC ACID
AP1	2-NITRATOMETHYL-6-METHYL-PHENOL
AP2	2-METHYL-2-HYDROXY-5-HEPTYLNITRATE
AP3	3-METHYL-4-HEPTYLNITRATE
AP4	1,2-DIMETHYL-3-METHYLNITRATO-BENZENE
AP5	4-METHYLNITRATO-BENZALDEHYDE
AP6	4-METHYLNITRATO BENZOIC ACID
AP7	1-METHYL-1-NITRATO-2,3-DIHYDROXY-4-ISOPROPYL-CYCLOHEXANE
AP8	1-METHYL-4-NITRATO-4-ISOPROPYL-5-HYDROXY-CYCLOHEXENE
AP9	5-ISOPROPYL-6-NITRATO-4-HEXEN-2-ONE
AP10	1-METHYL-2-METHYLNITRATO-NAPHTHALENE
AP11	8-HEXADECYLNITRATE
AP12	8-HYDROXY-11-HEXADECYLNITRATE
UR1	3-METHYL-HEPTANOIC ACID
UR2	3-HYDROXY-4-METHYL BENZOIC ACID
UR3	2-HYDROXY-3-ISOPROPYL-6-OXO-HEPTANOIC ACID
UR4	2-ISOPROPYL-5-OXO-HEXANAL
UR5	1-METHYL-3-HYDROXY-4-ISOPROPYL-1,2-CYCLOHEXANE EPOXIDE
UR6	2-HYDROXY-3-ISOPROPYL-6-METHYL-CYCLOHEXANONE
UR7	3,7-DIMETHYL-6-OXO-3-OCTENAL
UR8	3-ISOPROPYL-6-OXO-3-HEPTENOIC ACID
UR9	1-METHYL-4-ISOPROPYL-1,2CYCLO-4-HEXENE EPOXIDE
UR10	3-ISOPROPYL-6-METHYL-3-CYCLOHEXENONE
UR11	1,2-DIMETHYL-3-HYDROXY-NAPHTHALENE
UR12	1,2,3-TRIMETHYL-5-NITRO-BENZENE
UR13	3-n-PROPYL-4-NITRO-TOLUENE
UR14	2-NITRO-4-METHYL-BENZOIC ACID
UR15	1,2-DIMETHYL-3-NITRO-NAPHTHALENE
UR16	2-METHYL-2-HYDROXY-5-HEPTANONE
UR17	2-HYDROXY-3-ISOPROPYL-HEXADIAL
UR18	3-ISOPROPYL-2-PENTENDIAL
UR19	1-METHYL-2-FORMYL-NAPTHALENE
UR20	11-HYDROXY-8-HEXADECANONE
UR21	KETO-PROPANOIC ACID
UR22	2,6-DIMETHYL-3,4-DINITRO-PHENOL
UR23	3-ISOPROPYL-4-HYDROXY-2-BUTENOIC ACID
UR24	MALEIC ANHYDRIDE
UR25	3H-FURAN-2-ONE
UR26	4,5-DIMETHYL-6-OXO-2,4-HEPTADIENOIC ACID
UR27	2-CARBOXY-ACETOPHENONE
UR28	OXALIC ACID
UR29	4-HYDROXY-3,5-DIMETHYL-2,4-HEXADIENDIOIC ACID
UR30	2-METHYL-5-CARBOXY-2,4-HEXADIENDIOIC ACID
UR31	2-(DIMETHYL-PROPENOIC ACID)-BENZOIC ACID
UR32	3-METHYL-4-HEPTANONE
UR33	2-ISOPROPYL-5-OXO-2-HEXENAL
UR34	8-HEXADECANONE

Table A.2: Gas-phase chlorine chemistry mechanism: rate constants are given $k = \mathbf{A} / T \times \exp(\mathbf{E/R}T)$ in ppm min^{-1}, where T is the ambient temperature in K.

Reaction			A	E/R	Reference	
$HOCl + h\nu$	→	$OH + Cl$				Photolysis
$Cl_2 + h\nu$	→	$Cl + Cl$				Photolysis
$ClNO + h\nu$	→	$Cl + NO$				Photolysis
$ClNO_2 + h\nu$	→	$Cl + NO_2$				Photolysis
$ClONO_2 + h\nu$	→	$0.9\ Cl + 0.9\ NO_3 + 0.1\ ClO + 0.1\ NO_2$				Photolysis
$OClO + h\nu$	→	$ClO + O(^3P)$				Photolysis
$ClONO + h\nu$	→	$Cl + NO_2$				Photolysis
$HCOCl + h\nu + O_2$	→	$Cl + HO_2 + CO$				Photolysis
$Cl_2 + OH$	→	$Cl + HOCl$	1.59e+6	-1200	*Atkinson et al.*, 2000	
$Cl + OClO$	→	$ClO + ClO$	1.41e+7	700	*Atkinson et al.*, 2000	
$Cl + O_3$	→	$ClO + O_2$	1.28e+7	-260	*Atkinson et al..*, 2000	
$Cl + H_2 + O_2$	→	$HCl + HO_2$	1.72e+7	-2310	*Atkinson et al..*, 2000	
$Cl + H_2O_2$	→	$HCl + HO_2$	4.85e+6	-980	*Atkinson et al..*, 2000	
$Cl + HO_2$	→	$HCl + O_2$	7.93e+6	170	*Atkinson et al..*, 2000	
$Cl + HO_2$	→	$ClO + OH$	1.81e+7	-450	*Atkinson et al..*, 2000	
$Cl + HOCl$	→	$Cl_2 + OH$	1.10e+6	-130	*DeMore et al.*, 1997	
$ClO + O_3$	→	$Cl + 2\ O_2$	6.61e+0		*Atkinson et al.*, 2000	upper limit @ 298 K
$ClO + O_3$	→	$OClO + O_2$	4.40e–1		*Atkinson et al.*, 2000	upper limit @ 298 K
$ClO + HO_2$	→	$HOCl + O_2$	2.03e+5	710	*Atkinson et al.*, 2000	
$ClO + ClO$	→	$Cl_2 + O_2$	4.40e+5	-1590	*Atkinson et al.*, 2000	
$ClO + ClO$	→	$Cl + Cl + O_2$	1.32e+7	-2450	*Atkinson et al.*, 2000	
$ClO + ClO$	→	$Cl + OClO$	1.54e+5	-1370	*Atkinson et al.*, 2000	
$ClO + OH$	→	$0.93\ Cl + 0.93\ HO_2 + 0.07\ HCl + 0.07\ O_2$	3.39e+6	270	*Atkinson et al.*, 2000	
$OClO + OH$	→	$HOCl + O_2$	1.98e+5	800	*Atkinson et al.*, 2000	
$HCl + OH$	→	$Cl + H_2O$	7.93e+5	-240	*Atkinson et al.*, 2000	
$HOCl + OH$	→	$ClO + H_2O$	2.20e+5		*Atkinson et al.*, 2000	
$ClO + SO_2$	→	$Cl + SO_3$	1.76e+0		Estímate	
$Cl + ClNO + M$	→	$ClNO + M$	function		*DeMore et al.*, 1997	
$Cl + ClNO$	→	$Cl_2 + NO$	2.55e+7	100	*DeMore et al.*, 1997	
$Cl + NO_2 + M$	→	$ClONO + M$	function		*DeMore et al.*, 1997	
$Cl + NO_2 + M$	→	$ClNO_2 + M$	function		*DeMore et al.*, 1997	
$Cl + NO_3$	→	$ClO + NO_2$	1.06e+7		*Atkinson et al.*, 2000	
$Cl + HNO_3$	→	$HCl + NO_3$	8.81e+1		*Atkinson et al.*, 2000	upper limit @ 298 K
$Cl + ClONO_2$	→	$Cl_2 + NO_3$	2.86e+6	135	*Atkinson et al.*, 2000	
$ClO + NO$	→	$Cl + NO_2$	2.73e+6	295	*Atkinson et al.*, 2000	
$ClO + NO_2 + M$	→	$ClONO_2 + M$	function		*DeMore et al.*, 1997	
$ClO + NO_3$	→	$0.74\ Cl + NO_2 + 0.74\ O_2 + 0.26\ OClO$	2.03e+5		*Atkinson et al.*, 2000	
$HCl + NO_3$	→	$Cl + HNO_3$	2.20e+1		*Atkinson et al.*, 2000	upper limit @ 298 K
$ClNO_2 + OH$	→	$HOCl + NO_2$	1.06e+6	-1250	*Atkinson et al.*, 2000	
$OClO + NO$	→	$ClO + NO_2$	1.50e+5		*Atkinson et al.*, 2000	
$ClNO + OH$	→	$HOCl + NO$	3.96e+6	-1130	Estimated	
$ClNO + OH$	→	$Cl + HONO$	4.05e+4	240	Estimated	

Table A.2 (cont.): Gas-phase chlorine chemistry mechanism: rate constants are given $k = \mathbf{A} / T \times \exp(\mathbf{E/R}T)$ in ppm min^{-1}, where T is the ambient temperature in K.

$Cl + CH_4$	→	$HCl + RO21 + RO2T$	4.23e+6	-1360	*Sander et al.*, 2000	
Cl + ALKL	→	HCl + RO25 + RO2T	9.69e+7		*Atkinson*, 1997	Using 2-dimethylbutane via SSR and Table 3 of *Atkinson*, 1997
Cl + ALKM	→	HCl + RO220 + RO2T	1.76e+8		*Atkinson*, 1997	Using 3,5 dimethylheptane via SSR
Cl + ALKH	→	HCl + RO232 + RO2T	3.96e+8		*Atkinson*, 1997	Using n-hexadecane via SSR
$Cl + HCHO$	→	$HCl + HO_2 + CO$	3.66e+7		*Atkinson et al.*, 1999	
Cl + ALD2	→	HCl + RO26 + RO2T	5.29e+7		*Atkinson et al.*, 1999	Using propanal (C2H5CHO) value (n-pentanal (*) not available / found)
$Cl + MeOH$	→	$HCl + HCHO + HO_2$	2.42e+7		*Atkinson et al.*, 1999	
$Cl + EtOH$	→	$HCl + ALD2 + HO_2$	3.96e+7		*Atkinson et al.*, 1999	
Cl + ALCH	→	HCl + RO22 + RO2T	6.61e+7		*Atkinson et al.*, 1999	Using n-propanol (n-C3H7OH) Value (2-hexanol value not available / found
Cl + MTBE	→	HCl + RO215 + RO2T	6.17e+7		*Notario et al.*, 2000a	
Cl + MEK	→	HCl + RO27 + RO2T	3.08e+7		*Notario et al.*, 2000b	Using 3-methyl-2-butanone Value (2-pentanone value not available / found)
Cl + KETO	→	HCl + RO216 + RO2T	4.85e+7		*Notario et al.*, 2000b	Using 5-methyl-2-hexanone Value (2-heptanone value not available / found)
Cl + ETHE	→	CLRO21 + RO2T	1.72e+6	966	*Coquet and Ariya*, 2000	Using value from *Coquet and Ariya*, 2000 with Erratum
Cl + OLEL	→	CLRO22 + RO2T	1.76e+7	745	*Coquet and Ariya*, 2000	Using 1-pentene value from *Coquet and Ariya*, 2000 with Erratum
Cl + OLEH	→	CLRO23 + RO2T	1.76e+7	745		Using same value as above (no higher alkene data found)
$CLRO21 + NO$	→	$NO_2 + HCHO + CLRO24 + RO2T$				Using same value as reaction 113 (RO22 + NO): *Griffin et al.*, 2002a
$CLRO21 + HO_2$	→	$OH + HCHO + CLRO24 + RO2T$				Using same value as reaction 94: *Griffin et al.*, 2002a
CLRO21 + RO2T	→	$O_2 + HCHO + CLRO24 + RO2T + ALD2 + HO_2$				Using same value as reaction 96: *Griffin et al.*, 2002a
$CLRO22 + NO$	→	$NO_2 + ALD2 + CLRO24 + RO2T$				Using same value as reaction 113 (RO22 + NO) : *Griffin et al.*, 2002a
$CLRO22 + HO_2$	→	$OH + ALD2 + CLRO24 + RO2T$				Using same value as reaction 94: *Griffin et al.*, 2002a
CLRO22 + RO2T	→	$O_2 + ALD2 + CLRO24 + RO2T + ALD2 + HO_2$				Using same value as reaction 96: *Griffin et al.*, 2002a
$CLRO23 + NO$	→	$NO_2 + ALD2 + CLRO24 + RO2T$				Using same value as reaction 170 (RO218 + NO) : *Griffin et al.*, 2002a
$CLRO23 + HO_2$	→	$OH + ALD2 + CLRO24 + RO2T$				Using same value as reaction 94: *Griffin et al.*, 2002a
CLRO23 + RO2T	→	$O_2 + ALD2 + CLRO24 + RO2T + ALD2 + HO_2$				Using same value as reaction 96: *Griffin et al.*, 2002a
$CLRO24 + NO$	→	$NO_2 + HCOCl + HO_2$				Using same value as reaction 95: *Griffin et al.*, 2002a
$CLRO24 + HO_2$	→	$OH + HCOCl + HO_2$				Using same value as reaction 94: *Griffin et al.*, 2002a
CLRO24 + RO2T	→	$O_2 + HCOCl + HO_2 + RO2T$				Using same value as reaction 96: *Griffin et al.*, 2002a
Cl + RO21	→	$ClO + HCHO + HO_2$	3.52e+7		*DeMore et al.*, 1997	based on *Maricq et al.*, 1994
Cl + RO21	→	HCl + CRIEG1	3.52e+7		*DeMore et al.*, 1997	based on *Maricq et al.*, 1994
Cl + RO25	→	HCl + CRIEG2	3.39e+7		*DeMore et al.*, 1997	based on *Maricq et al.*, 1994
Cl + RO25	→	$ClO + ALD2 + HO_2$	3.26e+7		*DeMore et al.*, 1997	based on *Maricq et al.*, 1994
$ClO + RO21$	→	$Cl + HCHO + HO_2 + O_2$	1.46e+6	-115	*DeMore et al.*, 1997	
$CRIEG1 + NO$	→	$HCHO + NO_2$	3.08e+6		Estimated	
$CRIEG1 + NO_2$	→	$HCHO + NO_3$	3.08e+5		Estimated	
$CRIEG1 + H_2O$	→	ACID	1.76e+0		Estimated	
$CRIEG2 + SO_2$	→	$ALD2 + SO_3$	3.08e+4		Estimated	
$CRIEG2 + NO$	→	$ALD2 + NO_2$	3.08e+6		Estimated	
$CRIEG2 + NO_2$	→	$ALD2 + NO_3$	3.08e+5		Estimated	
$CRIEG2 + H_2O$	→	ACID	1.76e+0		Estimated	
Cl + ISOP + *NO*	→	NO2 + 0.42 HCOCL + 0.21 MVK + 0.21 MCR + 0.58 HO_2 + 0.29 CLI1 + 0.29 CLI2	2.25e+8		Estimated	Products: personal communication with Dr. Barbara J. Finlayson-Pitts
$HNO_3 + hv$	→	$OH + NO_2$				Photolysis

Appendix B: Sea-salt derived Cl_2 and $ClNO_2$ fluxes

Four files are attached to the electronic version of this report:

ss1arbflxs08.zip – Case Cl Chem, September 8, 1993

ss1arbflxs09.zip – Case Cl Chem, September 9, 1993

ss2arbflxs08.zip – Case Cl Chem & NO_3 Reaction, September 8, 1993

ss2arbflxs09.zip – Case Cl Chem & NO_3 Reaction, September 9, 1993

These files contain the hourly averaged molecular chlorine (Cl_2) and nytryl chloride fluxes ($ClNO_2$) due to heterogeneous reactions on sea-salt particles within the computational domain.

The data contained within the files can be read with the following FORTRAN format statement: FORMAT(3(I2, 1X), 10(E12.4, 1X)). The integer fields denote the initial time, horizontal coordinate and vertical coordinate, respectively. The first five real fields denote the Cl_2 flux for each of the five vertical levels of the model, respectively. Similarly, the second set of five real fields denotes the $ClNO_2$ flux per vertical level. The units of the flux rates are in ppm/min. The heights of the computational cells, measured from local ground level, are 12.98 m, 52.69 m, 153.89 m, 330.11 m and 550.33 m.

The horizontal and vertical coordinates are given with respect to the master domain:

Master Domain Computational Domain (400 km x 150 km)

UTM Coordinates - (Easting, Northing) Zone 11: (210, 3680) to (610, 3830)

5 km x 5 km resolution,

80 horizontal x 30 vertical cell grid